Bulletin of the New Zealand Society for Earthquake Engineering, Vol. 55, No. 3, September 2022

SYSTEM OVERSTRENGTH FACTOR INDUCED BY INTERACTION BETWEEN STRUCTURAL REINFORCED CONCRETE WALLS, FLOORS AND GRAVITY FRAMES-ANALYTICAL FORMULATION

Reza E. Sedgh[1], Rajesh P. Dhakal[2], Chin-Long Lee[3] and Athol Carr[4]

(Submitted *October 2020;* Reviewed *February 2021*; Accepted *November 2021*)

ABSTRACT

In multi-storey structural wall buildings, the structural walls are required to resist additional shear force due to their interactions with the floors and gravity-resisting system, which is not fully catered for in current seismic design provisions and assessment guidelines. This paper scrutinizes the mechanics of the interaction between structural reinforced concrete (RC) structural walls, floors and gravity frames in multi-storey RC structural wall buildings during elastic and nonlinear response phases. It also investigates the implications of this interaction on design of multi-story RC wall buildings. Generic expressions are derived to predict the drift and rotation profiles of multi-storey RC wall buildings. Then, a simple hand calculation method is developed to estimate the system (moment) overstrength of multi-storey RC wall buildings due to system (wall-floor-frames) interaction. The proposed method is applied to a prototype building with different slab dimensions and stiffness, and verified by comparing with the system overstrength factor obtained using finite element analysis. The simplified method estimates, and the nonlinear finite element analyses results agree, that a system overstrength factor of 1.7 can be used to account for the 3D interaction between the structural walls, floors and gravity frames in design and assessment of typical ductile RC wall buildings.

INTRODUCTION

Reinforced concrete (RC) structural walls are commonly used in conjunction with various floor systems to resist earthquake actions. While precast pre-stressed flooring systems made of double tee, rib and in-fill, and hollow core (until very recently) units are more commonly used than other flooring systems in New Zealand, two-way concrete flat slabs (in-situ or post-tensioned) are more common in many seismically active countries. Even in New Zealand, many existing pre-1970s buildings were constructed with this type of flooring system.

In typical building seismic design practice, the contribution of floor systems (such as two-way flat slabs) to the overall stiffness or strength of the building is often neglected because the main focus in seismic design is the performance of lateral-load-resisting systems. While the floor systems tie the lateral load resisting components together and provide diaphragm actions, they also act as a source of inertial and gravity loads. In regular structural wall buildings too, the seismic design demands on the structural walls are estimated considering the walls as decoupled components without properly accounting for the floors and gravity resisting components of the building. One of the main reasons for this is because the three-dimensional (3D) interaction between floor systems, structural walls and gravity systems has not yet been quantified in a simple enough manner for everyday design application.

The need to revisit design provisions for RC structural walls following evidences of unexpected performances of RC wall buildings in recent earthquakes [1,2] has been emphasized by multiple researchers [3-5]. This has led to more research [on RC walls with an aim to better understand and improve the seismic performance of RC walls [6-10]. These efforts have resulted in evidence-backed recommendations on improved design procedures for RC walls [11-14]. Nevertheless, these recommendations address issues related to seismic performance of isolated RC walls. The design implications of the complex 3D system interaction between structural walls and gravity columns through floor slabs has not attracted much attention in recent years.

In the past, several researchers attempted to experimentally and numerically investigate seismic performance of RC structural wall building systems to better understand the 3D interaction between structural walls, floor slabs and gravity frames. By performing shake table tests on multi-storey wall-frame buildings, significant contribution of the flooring system (two-way slabs) to the ultimate lateral strength of the tested buildings has been confirmed by multiple researchers [15-17]. These researchers found that axial growth and rocking at the base of structural walls (due to neutral axis movement) activate a three-dimensional outrigging action in the surrounding RC gravity frames. They concluded that this 3D effect introduces extra overstrength to the system (also known as kinematic overstrength), which highly depends on the level of drift that can be achieved at the ultimate limit state.

Panagiotou et al. [18] conducted an experimental investigation comprising a shake table test of a slice of a multi-storey RC wall building including floor slabs and gravity columns. They noted that the base moment resistance of the tested system at DBE (design basis earthquake) level shaking comprised three major components: (i) 55% from the web wall moment capacity; (ii) 32% due to coupling of the web through the slotted slabs; and (iii) 10% due to axial forces in the perpendicular gravity columns.

Furthermore, Henry et al. [19] demonstrated that lateral load response of buildings consisting of rocking walls can dramatically alter when the wall-to-floor interaction is accounted for, as they measured up to 50% increase in the

[1] *Corresponding Author, Senior Structural Engineer, MBIE, New Zealand reza.sedgh@mbie.govt.nz (Member)*
[2] *Professor, Department of Civil and Natural Resource Engineering, University of Canterbury, New Zealand rajesh.dhakal@canterbury.ac.nz (Fellow)*
[3] *Senior Lecturer, Department of Civil and Natural Resource Engineering, University of Canterbury, New Zealand chin-long.lee@canterbury.ac.nz*
[4] *Professor Emeritus, Department of Civil and Natural Resource Engineering, University of Canterbury, New Zealand athol.carr@canterbury.ac.nz*

lateral strength of the tested specimen at design level of lateral drift.

Gavridou et al. [20] modelled and analysed a full-scale four-storey un-bonded post-tensioned (UPT) concrete wall building that was tested under shake table excitation. They pointed out that displacement incompatibilities existed between the UPT beams, the floor system and the structural walls. Their analytical study demonstrated that the total moment resistance of the building in the direction of the concrete walls at the instant of peak strength during its response to a Kobe-earthquake ground motion was attributed to the following sources: 50% from the moment capacity of the UPT walls, 35% from the frame action of the UPT beams, 5% from the column base moments and the remaining 10% from the interior one-bay frame. Later, Watkins et al. [21] analysed the same test building using a more rigorous 3D model and reaffirmed that dynamic loading and wall-to-floor interaction significantly increase the over-strength actions compared to the overstrength developed when considering the wall system in isolation.

A precise estimation of the system overstrength factor in multi-storey buildings is difficult since many factors contribute to it. Many researchers have endeavoured to recognize the main contributors to overstrength in different structural systems [22,23]. It has been found that inherent randomness and uncertainties in major parameters such as actual strength of materials, confinement effects, contribution of non-structural elements, and participation of secondary structural elements (such as RC floor slabs) lead to large variations in the estimation of overstrength [24]. To acknowledge such unavoidable variations, a conservative overstrength factor (R_s) of 2.0 has been suggested for medium and low period RC buildings based on the results of studies on twelve RC buildings [25] designed and detailed in accordance with Eurocode 8 [26].

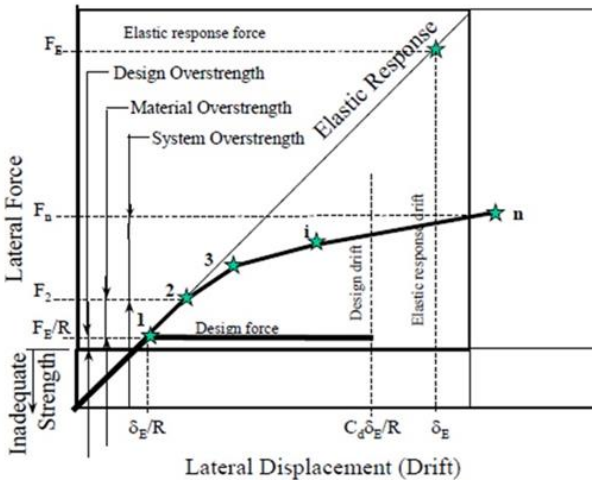

Figure 1: Factors affecting overstrength of a building system (FEMA-450 [27]).

According to FEMA-450 [27], basic components of structural overstrength (Ω_0) consist of material overstrength (Ω_M), system overstrength (Ω_S) and design overstrength (Ω_D). These components of overstrength are presented schematically in Figure 1. This study focuses on understanding and quantifying the effect of structural wall-slab-column interaction on the system overstrength (Ω_S) factor in typical multi-storey structural wall buildings. Note that system overstrength (Ω_S) is the ratio of the ultimate lateral force the structure is capable of resisting, F_n in Figure 1, to the actual force at which the first significant yield occurs, F_2 in Figure 1. It is dependent on the extent of redundancy contained in the structure as well as any probable contribution of secondary components in resisting the lateral force. Redistribution of internal actions after ductile yielding in critical zones is another key contributor to this overstrength.

The fundamental objective of capacity design is to restrict the inelastic mechanism in well-detailed ductile regions via a strength hierarchy. In case of structural RC wall buildings, the design intent is to resist seismic actions and dissipate seismic energy through the formation of plastic hinges at the base of shear walls while the floor diaphragms vertically supported by a combination of structural walls and gravity columns remain elastic (or in specific cases a certain degree of cracking is allowed without yielding). It is to be noted here that in capacity design the effects of overstrength are not always beneficial. For example, the flexural overstrength of members leads to increased shear forces when plastic hinges form, which may result in non-ductile failure. Therefore, any possible source of overstrength in a building should be taken into consideration in capacity design. While amendments to several aspects of current NZ design and detailing provisions for structural RC walls have recently been recommended [11], the requirement to account for the aforementioned system interaction was not included in these recommendations.

To meet the capacity design requirements for RC structural walls as per NZ concrete design standards (NZS 3101:2006 [28]), the design shear force (V^*_{wall}) at any level above the plastic hinge shall not be taken less than the corresponding shear force found from the equivalent static analysis multiplied by a section overstrength factor (φ_o) and a dynamic shear magnification factor (ω_v) such that:

$$V^*_{wall} = \omega_v \varphi_o V^*_E \quad (1)$$

In the above equation, ω_v is a function of the period of the structural wall and φ_o is the sectional overstrength of the plastic hinge zone at the wall base under flexural actions. While the sources and consequences of the overstrength factor are scrutinised in detail in this paper, the effect of dynamic amplification is not considered to enable quantifying the isolated effect of 3D spatial interaction on the system response.

In this paper, the mechanism of 3D (spatial) interaction between floor systems, structural RC walls and gravity frames leading to the ability of structural wall building systems to resist additional demand (i.e. overstrength) is discussed first. Then, a simplified method to account for the system overstrength factor is proposed. Finally, to verify the proposed method and to quantify the effect of floor characteristics on the system response of multi-storey RC structural wall buildings, the system overstrength of five different typical buildings with varying floor (i.e. bay) length and floor stiffness are estimated by employing the proposed simplified method and finite element analyses.

The main research questions addressed in this paper are:

(1) Which variables/parameters play a significant role in 3D interaction between the floors, structural walls and gravity frames?

(2) How much do the out-of-plane flexural stiffness of two-way floor slabs and bay (i.e. floor) length affect the lateral strength of multi-storey RC wall buildings?

(3) Can a mechanics-based simplified procedure be developed to reasonably estimate the system overstrength of multi-storey RC wall buildings without having to conduct a complex 3D nonlinear finite element analysis?

(4) What system overstrength factor shall be used in design to account for the wall-floor-frame interaction in typical ductile multi-storey RC structural wall buildings?

(5) Can generic equations be developed to predict the interstorey drift ratios along the height of multi-storey RC structural wall buildings?

In order to answer the abovementioned research questions, the following assumptions and simplifications are made in this research:

- Nonlinearity is limited to the base plastic hinge of RC structural walls. Although wall-floor-frame interactions can alter the strength hierarchy and lead to different failure modes, all other failure mechanisms (such as wall-floor or columns-floor connections) are suppressed across the analysis to allow the wall to develop full overstrength.
- The effective floor stiffness (cracked) is isotropic and uniform throughout the floor. Note that while this assumption is well justified for two way concrete flat slabs (with or without prestressing), but it will slightly overestimate the floor contribution in precast floors made of single/double tee, hollow-core, rib and raft systems as such floors have weaker cross section profile in the transverse direction.
- To isolate the effect of floor systems, flexural behavior of gravity columns is neglected in the analysis.
- The inevitable random variation of material strengths is assumed to affect all cases (isolated walls as well as wall-floor-frame system) equally. Hence, it is not considered in deriving the system overstrength factor.

THREE DIMENSIONAL SPATIAL INTERACTION MECHANISM

This section explains the mechanism related to wall-frame-slab interaction in the post-yielding (nonlinear) phase. A typical regular multi-storey structural wall building is designed for this purpose. This is because simple regular systems are deemed necessary to demystify the complex 3D issues addressed in this investigation. The simple and regular building configuration would also facilitate identifying and quantifying key variables that contribute most to the system response (and the overstrength factor) through extensive parametric analysis.

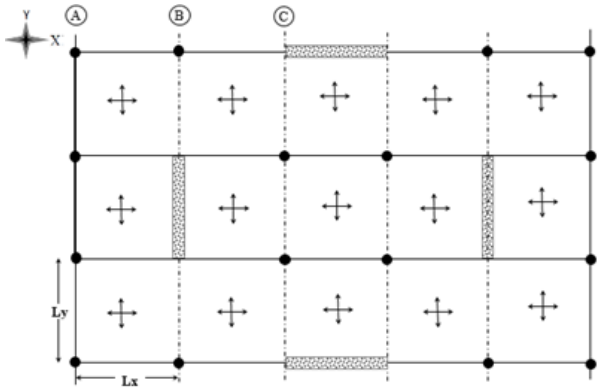

Building floor plan

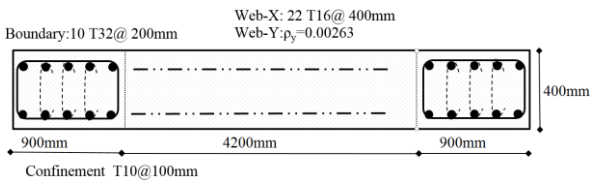

Wall base section

Figure 2: Building plan and the wall base section.

Floor plan of the building, the wall section details and the design information are illustrated in Figure 2 and Table 1. The building is eight-story high with 3.20 m story height and has a footprint dimension of 30 m by 18 m. The gravity system of the building consists of 200 mm thick RC slabs and circular (500 mm diameter) RC columns. The building is designed based on the design provisions defined in the NZ concrete structures standard [28] and the NZ loading standard [29]. The prototype building is assumed to be located in Wellington on Soil type C. The seismic mass of each floor is calculated as 4542.3 kN (Table 1). The natural period of the building is estimated by Eigenvalue analysis using stiffness values for all elements (columns, walls, and slabs) as recommended in NZS 3101:2006 [28].

Table 1: Building design information.

Rectangular wall section	6000 x 400 mm	Near fault factor	1
Typical floor height	3.20 m	Seismic weight on each floor	4542.3 kN
f_c f_{yl}, f_{yh}	30, 430*, 300 MPa	Soil type	C
Gravity columns diameter	500 mm	Z factor	0.4
Slab thickness	200 mm	Return period factor	1.0
Gravity load on each wall (base)	$0.08f_cA_g$	Structural ductility	5

* Grade 430 bars are not currently available in New Zealand, but were in common use in the past.

The deformation patterns of the building in the linear and nonlinear phases are demonstrated in Figure 3. These figures illustrate only the system behaviour in Y direction indicated in the building floor plan. The imposed lateral loads are based on the assumption that the wall acts as an isolated cantilever in pure bending with insignificant shear deformation. Note that the presence of floor slabs can arguably alter the wall's deformation profile, but the numerical analyses (presented later) showed that while the floor slabs slightly increase the initial (cracked) stiffness of the whole system their effect of on the wall deformation profile is localised and insignificant. The analysis also showed that while the deformation pattern remains predominantly in flexural mode, the presence of the floor slabs mainly changes the amount of moment demand on the RC structural walls at a given drift level.

Figure 4(a) shows a schematic deformation of a representative flooring system due to rocking (sectional rotation) of the structural wall in the other direction (i.e. X) [30]. Similarly, Figure 4(b) indicates how the deformation incompatibility between the wall (due to flexural deformation) and floor slab might force the surrounding elements to deform. Previous studies also showed that this mechanism can activate flexural and/or torsional actions within the floor systems [31]. The connections between the floor slabs and the structural walls significantly differ in construction practice due to variability in the flooring types. However, in this study typical rigid connections are assumed in both directions. This assumption implies that the floor slabs are provided with enough strength to continue resisting internal actions when the walls are pushed to develop their full moment capacity. Therefore, it should be acknowledged that if the floor slabs fail to carry the loads induced by the system interaction (such as out-of-plane actions), such buildings will perform differently and this assumption will lead to overestimation of the additional demand on walls. Nevertheless, equivalent flexural stiffness of the floor slabs used in the study accounts for the effect of cracking, which ensures that the forces induced by the floor deformation are realistic.

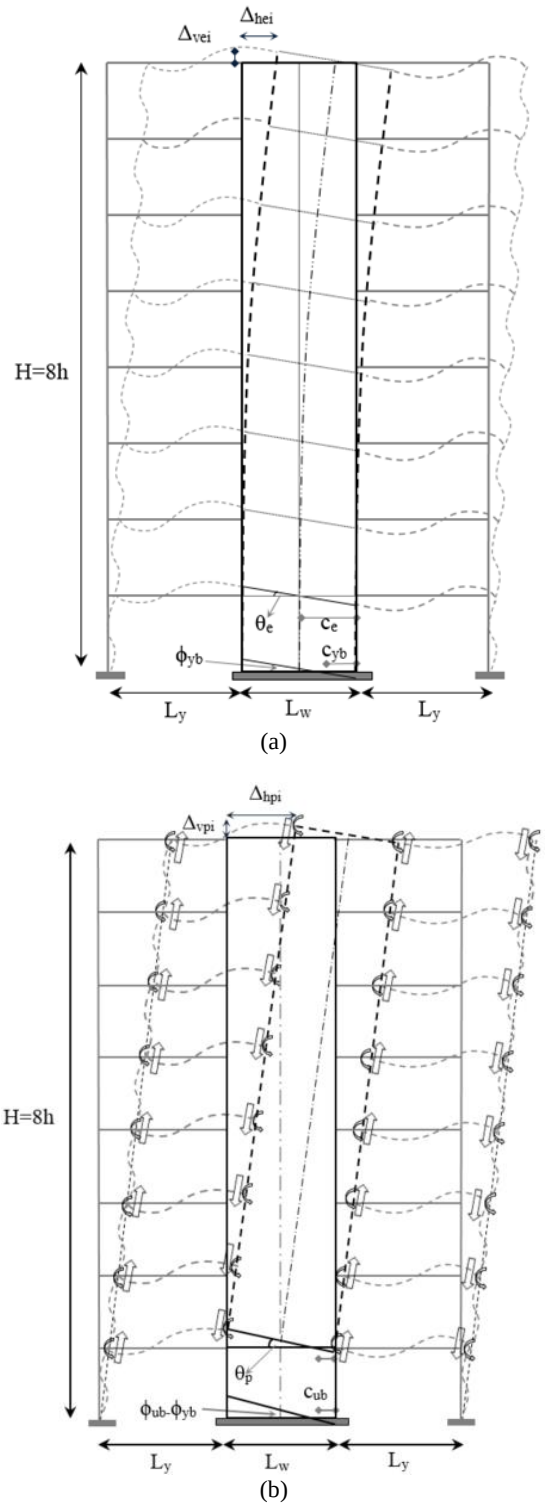

Figure 3: Elastic deformation due to elastic curvature (a); Plastic deformation due to plastic hinge rotation (b). [Note: The rotations have been amplified for clarity and are not intended to be to scale]

For a given applied force pattern over the building height, the two edges of the structural walls move vertically; due to the movement of neutral axis in monotonic loading and elongation (axial growth) of the wall in cyclic loading [32]. Although axial elongation in cyclic loading could force all longitudinal reinforcing bars in RC members (beams/columns/walls) to permanently stretch [33,34]; thereby resulting in both edges of a wall to move upwards, monotonic loading of a wall causes tension in only one edge while the other remains in compression. The edge of the wall in the tension side moves up (forcing the connected slab to displace upwards) and the edge in the compression side moves down (taking the slab downwards with it). The tensile edge elongation and compression edge shortening of the structural wall increase further in the post-elastic response phase; thereby activating the out-of-plane stiffness of the floor slabs (or other roofing/flooring systems). This interaction induces significant additional axial forces in the gravity columns connected to the floor slabs, which can develop extra moment capacity in the system. Moreover, the axial forces induced in the gravity columns are more pronounced when the wall starts yielding and enters the post-elastic range. In a ductile structure, the floor system (or flat floor slabs in this case study) will almost always be required to remain elastic, so that they can sustain their function of transferring seismic forces to the main lateral load resisting elements, and tying the building together. Therefore, diaphragms (floor slabs) should in principle have the strength to sustain the maximum forces that may be induced in them for a chosen yielding mechanism within the rest of the structure. As no elements (other than the structural walls) in the building are designed to resist shear, any additional shear force generated due to this interaction is required to be resisted by the structural walls themselves. The implication is that, shear force demand on the structural wall in different stories will be increased and this can impact the hierarchy of the failure mechanism in ductile RC walls.

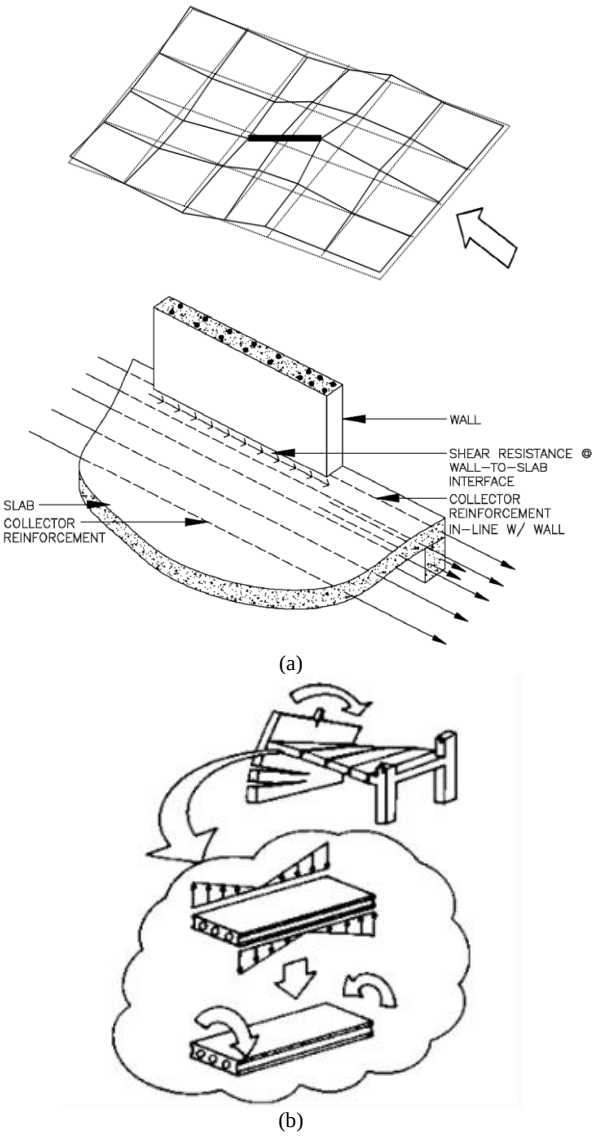

Figure 4: a) Floor deformation due to deformation incompatibility and slab to wall connection [30]; b) Deformation incompatibility of wall and surrounding slabs in a typical floor system [31].

DISTRIBUTION OF CURVATURE OVER THE HEIGHT

When the wall base section curvature equals the effective yielding curvature (equivalent to yielding of all reinforcement in the boundary element of the wall base section), the distribution of curvature over the height of the structural wall can be expressed as a function of the yielding curvature (see Figure 5). Although the distribution of lateral forces over the building height could be approximated using equivalent static analysis provisions, a linear lateral load pattern with zero intensity at the base is assumed over the building height in this study. For simplicity, the triangular lateral force profile and the cantilever deformation pattern of walls shown in Figure 5 ignore the inevitable minor changes caused by the wall's interaction with the floors (more prevalent in the wall's post-yielding response phase). Note that a linear function for lateral forces results in a quadratic shear profile, cubic moment (or curvature) profile, fourth order rotation profile and a fifth order displacement profile. Hence, a fifth-degree polynomial shape function is used to represent the elastic deformation profile across the height of a prismatic rectangular cantilever wall.

$$Y(Z = h_i) = aZ^5 + bZ^4 + cZ^3 + dZ^2 + eZ + f \quad (2)$$

Equation (2) can be used to correlate the roof displacement and floor rotations with the base curvature, which will facilitate derivation of a generic deformation profile for structural wall buildings. In this equation, $Z = h_i$ represents the height of floor *i* from the base of the building and *Y* is the lateral displacement. As mentioned earlier, the fifth order displacement profile leads to a linear increase of force intensity (i.e. triangular) across the height, and a smaller order polynomial functions are not admissible as they lead to unrealistic distribution of lateral forces or shear forces across the height of the wall. The six coefficients in this equation can be obtained by satisfying the geometric and force boundary conditions under the continuous linear load pattern.

The obvious boundary conditions are:

$$Y(0) = Y'(0) = 0,\ EI.Y''(H) = 0,\ EI.Y'''(H) = 0,$$
$$EI.Y''''(0) = 0,\ Y(H) = \Delta_{roof}$$

These boundary conditions imply that the displacement, rotation and lateral force intensity are zero at the base; and the moment and shear force are zero at the roof level, where the lateral displacement (Δ_{roof}) is known. Solving the constants using these boundary conditions, the deformation profile can be derived as a function of the roof displacement as:

$$Y(Z) = \frac{\Delta_{roof}}{11H^5}Z^5 - \frac{10\Delta_{roof}}{11H^3}Z^3 + \frac{20\Delta_{roof}}{11H^2}Z^2 \quad (3a)$$

$$Y'(Z) = \frac{5\Delta_{roof}}{11H^5}Z^4 - \frac{30\Delta_{roof}}{11H^3}Z^2 + \frac{40\Delta_{roof}}{11H^2}Z \quad (3b)$$

$$Y''(Z) = \frac{20\Delta_{roof}}{11H^5}Z^3 - \frac{60\Delta_{roof}}{11H^3}Z + \frac{40\Delta_{roof}}{11H^2} \quad (3c)$$

$$Y''(0) = \phi_{base} = \frac{40\Delta_{roof}}{11H^2} \rightarrow\rightarrow\rightarrow \Delta_{roof} = \frac{11H^2}{40}\phi_{base} \quad (3d)$$

Substituting for Δ_{roof} in Equation (3c), we obtain the generic equation for the curvature distribution as a function of the base curvature:

$$Y''(Z) = \phi(Z) = \frac{M(Z)}{EI(Z)} = \frac{\phi_{base}}{2H^3}Z^3 - \frac{3\phi_{base}}{2H}Z + \phi_{base} \quad (4)$$

Therefore, the curvature variation over the wall height can be estimated by employing Equation (4) when the curvature at the wall base reaches the effective yield curvature. Similarly, the wall rotation at each storey level can be estimated as:

$$Y'(Z) = \theta(Z) = \frac{\phi_{base}}{8H^3}Z^4 - \frac{3\phi_{base}}{4H}Z^2 + \phi_{base}Z \quad (5)$$

Equation (5) provides a generic method to estimate elastic inter-storey drifts in different floors of multi-storey wall buildings, which addresses the final research objective identified earlier. This enables rapid estimation of design demands on drift-sensitive non-structural components in RC wall buildings and so that designers can choose low-damage non-structural systems that can accommodate the required level of drift and ensure continued functionality at serviceability limit state. Even at ultimate limit state, the drift profile can be added by adding plastic rotation which is constant across the height.

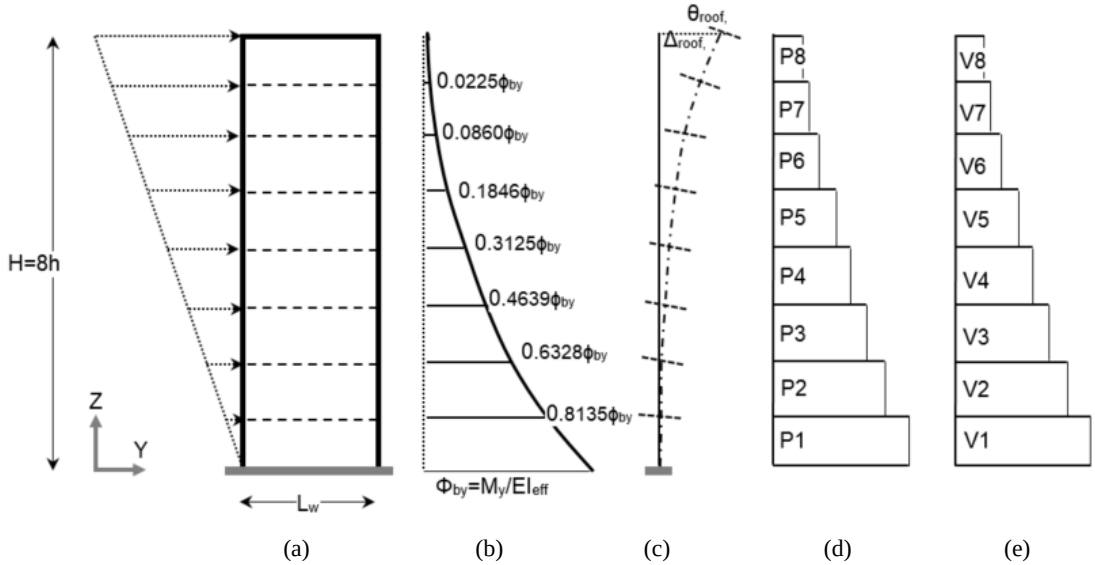

Figure 5: Height wise distribution of a) lateral force; b) curvature; c) flexural deformation and rotation; d) storey axial force; and e) storey shear force.

It is important to highlight that in reality, the lateral load distribution across the height of multi-storey buildings is not continuous; rather the forces are discretely applied at the floor levels. Hence, Equation (3d) may introduce some error when used to find a relation between the base curvature and roof displacement in a cantilever structural wall. For a given building height and base shear, different distributions of lateral forces can be applied over the building height depending on the distribution of mass in different floors. Figure 6 displays five different distributions of lateral forces over the building height

for a given base shear used to quantify the error incurred by assuming the lateral force profile to be continuous. To also investigate the effect of lateral force distribution pattern, the total base shear is distributed over the height of the building in two different ways. The first is a linear distribution according to New Zealand seismic action standard NZS 1170.5:2004 [29] (without the 8% lumped force at the roof level) and the second is proportional to the square of the height of a given floor from the base. These force distributions can be expressed respectively as:

$$F_i = \frac{h_i}{\sum_{i=1}^{n} h_i} \mathrm{V} \tag{6}$$

$$F_i = \frac{h_i^2}{\sum_{i=1}^{n} h_i^2} \mathrm{V} \tag{7}$$

where h_i is the height of floor i from the base. In the above equations, mass of all floors are assumed to be equal. The interrelation between the base curvature and roof displacement along with the corresponding correction factor for both force distributions are presented hereafter.

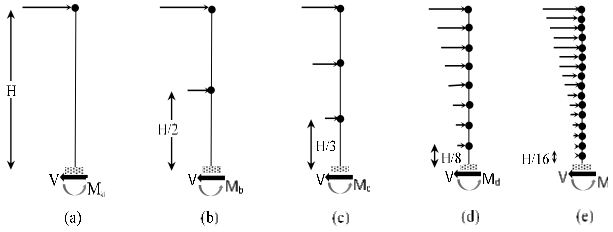

Figure 6: Different distributions of forces over the height.

As the fifth degree polynomial lateral displacement profile chosen earlier corresponds to a triangular (linear) continuous lateral force pattern, the interrelationship between the base curvature and the roof displacement derived using the assumed displacement profile would obviously be different from the one that corresponds to nonlinear distribution of discrete lateral forces. Nevertheless, the difference due to the linear and nonlinear profiles is likely to be small as the nonlinear force distribution profile does not deviate from a linear profile by a great extent. On the other hand, the error brought by the assumption of continuity depends on the number of floors in the building and can be significant for low-rise buildings with fewer stories. In this study, errors in the derived relationship due to both of these two sources are corrected via applying a correction factor.

Table 2 lists the actual relation between the base curvature and the roof displacement as well as the estimation error compared to a discrete load distribution. It is apparent that the error involved in employing Equation (3d) is reduced as the number of floors (n) increases. Hence, the correction factor to adjust Equation (3d) is defined as a function of number of stories (n). A regression analysis is performed to find the best fit curve. Figure 7 illustrates that the correction factor (λ) starts with the value of 0.8258 for a single-storey wall and it asymptotically approaches 1 as the number of stories increases. Thus, a modified form of Equation (3d) is proposed in Equation (8) by multiplying the original expression by the correction factor (λ) to account for the effects of nonlinearity and discreteness of the lateral force distribution.

Given the fact that most multi-storey shear wall buildings commonly have 5 or more storeys, the application of Equation (3d) will induce a maximum of 10% error. Hence, using Equation (3d) to estimate deformation profile of multi-storey wall buildings is justifiable for practical purposes; but Equations (8), (9) and (10) will provide a means to compensate for the error if/when needed.

$$\Delta_{roof} = \frac{11H^2}{40} \phi_{base} \times \lambda \tag{8}$$

$$\lambda = 1 - \frac{0.175}{n^{0.75}} \quad \text{linear force distribution} \tag{9}$$

$$\lambda = 1 - \frac{0.175}{n^{0.35}} \quad \text{parabolic force distribution} \tag{10}$$

It is interesting to note that the proposed simplified method is independent of the force applied to the system and relies on the base section effective yield curvature.

Table 2: Inter-relation between the base curvature and roof displacement (continuous load versus discrete load).

Case (Linear)	Δ_{roof}	Eq.(3d)	Error (%)	Correction factor (λ)
a(n=1)	$0.333\phi_{base}.H^2$	$0.275\phi_{base}.H^2$	21%	0.8250
b(n=2)	$0.308\phi_{base}.H^2$	$0.275\phi_{base}.H^2$	12%	0.8919
c(n=3)	$0.299\phi_{base}.H^2$	$0.275\phi_{base}.H^2$	8.7%	0.9199
d(n=8)	$0.285\phi_{base}.H^2$	$0.275\phi_{base}.H^2$	3.7%	0.9646
e(n=16)	$0.280\phi_{base}.H^2$	$0.275\phi_{base}.H^2$	1.9%	0.9813

Case (Parabolic)	Δ_{roof}	Eq.(3d)	Error (%)	Correction factor (λ)
a(n=1)	$0.333\phi_{base}.H^2$	$0.275\phi_{base}.H^2$	21%	0.8250
b(n=2)	$0.319\phi_{base}.H^2$	$0.275\phi_{base}.H^2$	16.2%	0.8609
c(n=3)	$0.312\phi_{base}.H^2$	$0.275\phi_{base}.H^2$	13.4%	0.8822
d(n=8)	$0.299\phi_{base}.H^2$	$0.275\phi_{base}.H^2$	8.7%	0.9200
e(n=16)	$0.293\phi_{base}.H^2$	$0.275\phi_{base}.H^2$	7.1%	0.9336

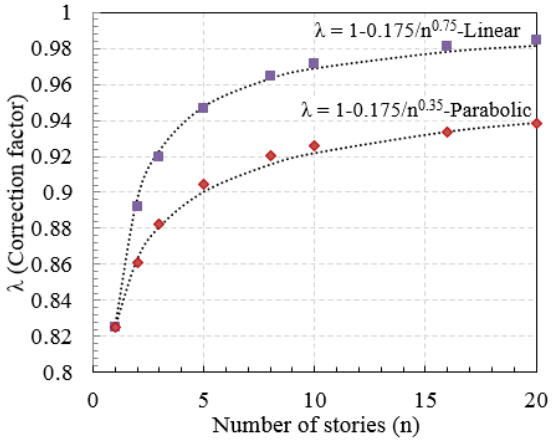

Figure 7: Correction factor for different distribution of forces over the height.

ESTIMATION OF EFFECTIVE YIELD CURVATURE AND NEUTRAL AXIS DEPTH

Another important variable is the neutral axis location at each storey level because the base neutral axis depth determines the centre of rotation once the RC wall rotates as a rigid block in the plastic phase. Due to inelastic behaviour of concrete in compression and its negligible strength in tension, the section neutral axis has to be positioned to satisfy the equilibrium between the axial load, the concrete compression force, and the compressive and tensile forces carried by the reinforcing bars. However, from the distribution of bending moment (which also resembles the curvature distribution until yielding), it can be confided that when the wall base section reaches the effective yield curvature, the section curvatures at upper storey levels are less than the effective yield curvature.

An extensive parametric section-analysis is conducted on various wall sections to investigate the variation of effective yield curvature (and equivalent neutral axis depth) in their moment-curvature responses. Moreover, this parametric study also investigates the variation of neutral axis depth when the sections reach their ultimate flexural strength. The effective yield curvature is determined using a standard moment-curvature analysis satisfying strain compatibility (using a linear strain profile across the section in line with the *plane section remains plane* assumption), material stress-strain relationships, and section equilibrium. Although the effective yield curvature of a section can change slightly due to the effects of tension stiffening and bond-slip, this study neglects them for brevity.

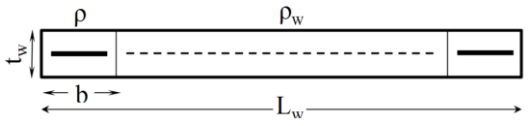

a) Section parameters

Parameters	Definition
L_w	Wall length
	4 m , 6 m , 8 m , 10 m
t_w	Wall thickness
	400 mm
b	Boundary length
	$0.1L_w$, $0.2L_w$
ρ	Boundary reinforcement ratio
	0.005-0.01-0.02-0.03
ρ_w	Web reinforcement ratio
	0.0025
$N/(A_g.f_c)$	Axial force ratio
	0.025-0.05-0.075-0.1
f_c	Concrete compressive stress
E_c	Concrete young's modulus
ε_c	Concrete peak strain
	30 MPa
	$Ec=5000\sqrt{f_c}=27386$ MPa
	0.003
f_y	Rebar yield strength
E_s	Rebar young's modulus
	430 MPa
	200000 MPa
cover	Distance to center of first rebar
	50 mm

b) Section analysis variables

Figure 8: Moment-curvature analysis and variables definition.

General features of the wall sections and the ranges of section variables included in the parametric analysis are shown in Figure 8. The longitudinal reinforcing bars in the boundary zone are spaced at 200 mm centres, and in the web they are assumed to be uniformly distributed to give the desired web reinforcement ratio (i.e. 2.5%). The stress-strain curve of concrete in compression is assumed based on the model proposed by Mander et al. [35], and an elasto-plastic stress-strain relationship is employed for reinforcing bars.

As shown in Figure 9, the effective yield curvature, ϕ_{yeff}, is obtained by extrapolating the first-yield curvature, ϕ_y to a point where the moment reaches the ultimate strength, M_u, assuming elasto-plastic response; i.e.

$$\phi_{yeff} = \frac{M_n}{M_y} \times \phi_y \quad (11)$$

where M_y is the moment resistance when the most extreme longitudinal rebar located in the boundary zone reaches ε_y (this condition holds true when the axial loads applied on the wall sections are relatively low) and the ultimate (nominal) flexural strength, M_n, is defined as the section moment capacity corresponding to the concrete strain of 0.003 at the extreme compression fibre.

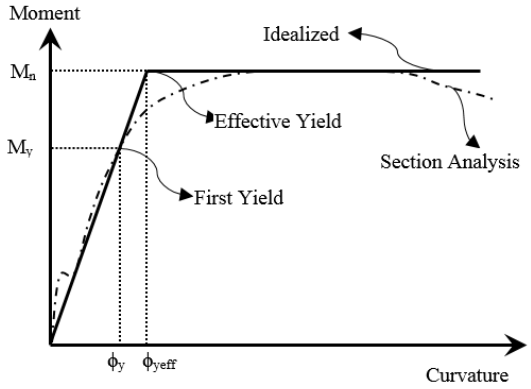

Figure 9: Definition of effective curvature in the section analysis.

Although multiple analyses were performed to estimate the effective yield curvature of rectangular wall cross sections for a given axial load and section geometry, only a few selected cases are presented here for brevity. Typical results of the parametric section analyses are shown in Figure 10 and Figure 11 for a rectangular wall section with a constant longitudinal web reinforcement ratio, concrete compressive strength and steel reinforcement yield strength. Each chart plots the effective yield curvature as a function of the axial load for different longitudinal boundary reinforcement ratios for a specified wall length (4 m in Figure 10 and 6 m in Figure 11) and a constant boundary zone length to wall length ratio (0.1 and 0.2). For known values of axial load, wall length, longitudinal boundary reinforcement ratio and longitudinal web reinforcement ratio, the effective yield curvature coefficient can be interpolated between the plotted curves. It is worth noting here that the bilinear idealization method based on Equation (11) introduces some error; especially in sections with low percentage of boundary reinforcement and low axial load ratios. For example, while the first yield curvature should decrease as the axial load ratio decreases, Figure 10 and Figure 11 show an opposite trend for axial load ratios less than 0.025 for most cases with 0.5 and 1 percent boundary reinforcement ratios.

However, it is desirable to develop a simplified formulation for rapid estimation of effective yield curvature without undertaking moment curvature analysis. Hence, the results of moment curvature analyses are herein compared with two simple expressions (Equations 12 and 13) proposed in the literature [36,37] that are commonly used for estimation of effective yield curvature. While both of these equations are independent of the applied axial force, the formulation in Equation (13) takes the effect of boundary reinforcement into account.

$$\phi_{yeff} = \frac{\varepsilon_y}{L_w} \times 2 \quad (12)$$

$$\phi_{yeff} = \frac{\rho_b^{0.07}}{L_w} \times 0.00534 \quad (13)$$

It is evident from Figure 10 and Figure 11 that Equation (12) consistently overpredicts the effective yield curvature in the presented cases. However, while Equation (13) also appears to slightly overestimate the effective yield curvature, within the typical range of axial forces ($0.025\text{-}0.075f_cA_g$) and boundary length ($0.2L_w$), its predictions match better (closer than

Equation 12) with the results of moment curvature analysis. Hence, it is reasonable to use Equation (13) for rapid estimation of effective yield curvature.

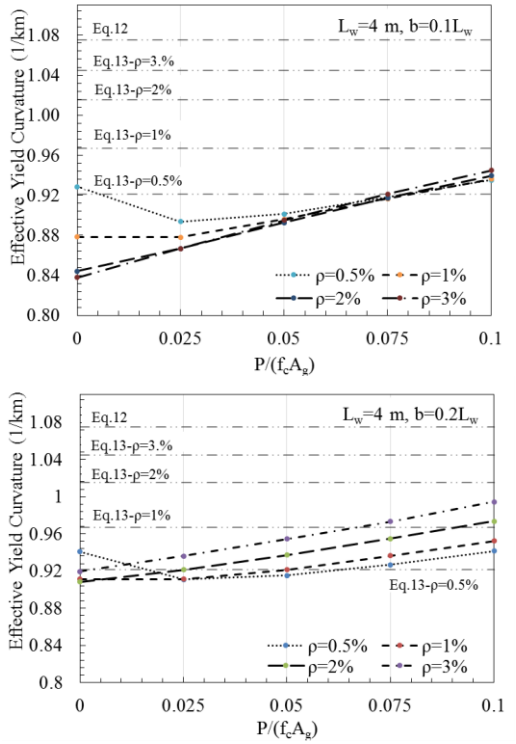

Figure 10: Variation of effective yield curvature with different parameters (L_w=4 m and b=0.1-0.2L_w).

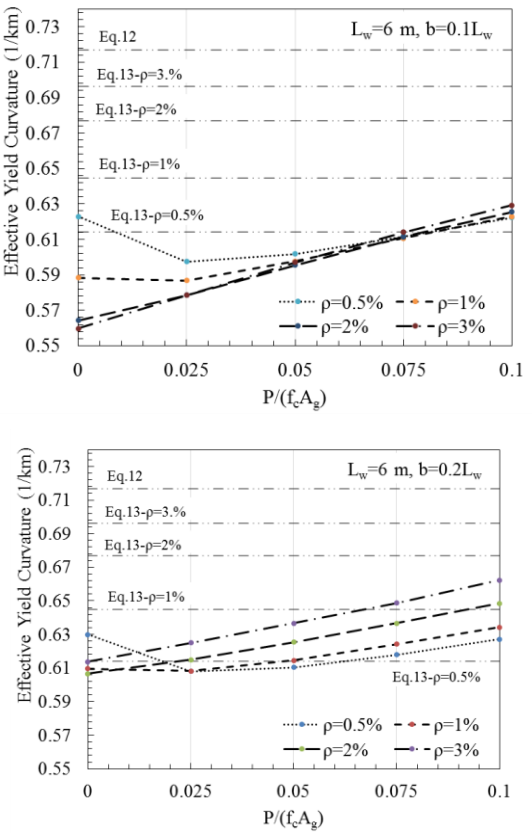

Figure 11: Variation of effective yield curvature with different parameters (L_w=6 m and b=0.1-0.2L_w).

Figure 12(a) shows the effective yield curvature versus axial load ratio for several wall sections analysed herein. Comparing the moment-curvature responses of different cases reveals that the effective yield curvature is significantly sensitive to the wall length for a given concrete and rebar strength. This is in line with findings of previous studies [36,37]. It is also observed that rectangular walls with different boundary zone lengths exhibit not too dissimilar results for the range of values covered in this study.

Figure 12(b) plots the neutral axis depth normalized with respect to the wall length when the section reaches its ultimate strength (i.e. corresponding to concrete crushing). It is evident that the normalized neutral axis depth (i.e. c_{ub}/L_w) varies between 0.05 to 0.2 depending on the amount of boundary zone reinforcement and the wall length. However, it is insensitive to the wall length. As the variation of neutral axis depth with respect to the wall length is minor, it cannot be distinguished in Figure 12(b).

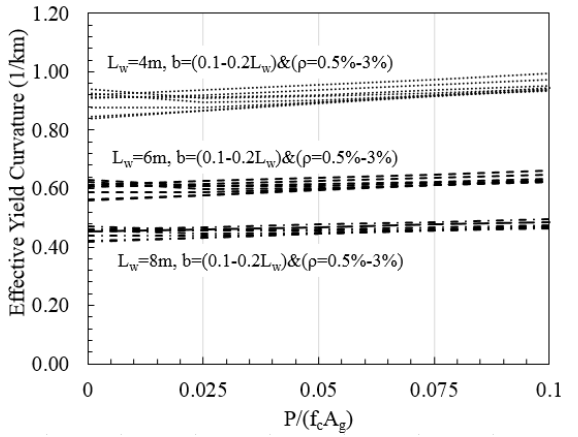

(a)

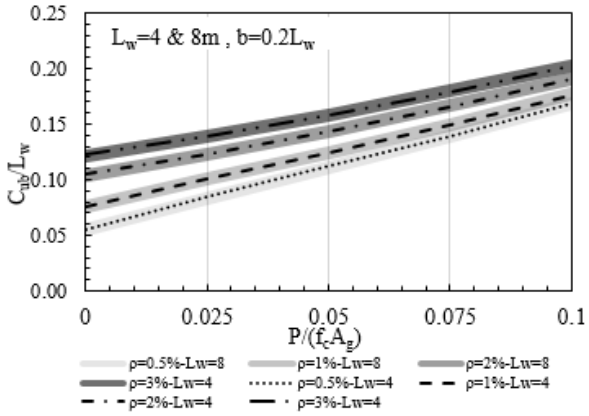

(b)

Figure 12: a) Effect of wall length on effective yield curvature b) Variation of neutral axis depth with different parameters at maximum flexural strength.

ESTIMATION OF VERTICAL DISPLACEMENTS OF WALL EDGES

Figure 13 demonstrates the procedure adopted herein to estimate the wall edge vertical displacements in the elastic and plastic states. When the curvature at the wall base equals the effective yield curvature, the deformed shape of the wall is shown in Figure 13(a). In this configuration, the vertical displacements at the left (tension) and right (compression) edges of the wall at each storey level are estimated by following the steps listed below,

- Calculate the effective yield curvature ϕ_{yeff} at the base section using Equation (11) or Equation (13).
- Calculate the elastic rotation at different storey levels by substituting $\phi_{base} = \phi_{yeff}$ in Equation (5).
- Calculate the vertical elastic displacements of the two wall edges at different storey levels as:

$$\Delta_{ve1(T)} = \Delta_{ve1(C)} = (\frac{L_w}{2}) \times \theta_{e1} \quad \text{at storey 1} \quad (14)$$

$$\Delta_{vei(T)} = \Delta_{vei(C)} = (\frac{L_w}{2}) \times \theta_{ei} \quad \text{at storey i} \quad (15)$$

where L_w is the wall length, and θ_{ei}, $\Delta_{vei(T)}$, and $\Delta_{vei(C)}$ are respectively the elastic rotation, the upward displacement of the tension edge, and the downward displacement of the compression edge at storey level *i*.

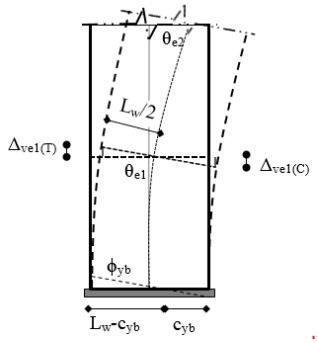

a) Elastic deformation of a wall when the base curvature reaches the effective yield

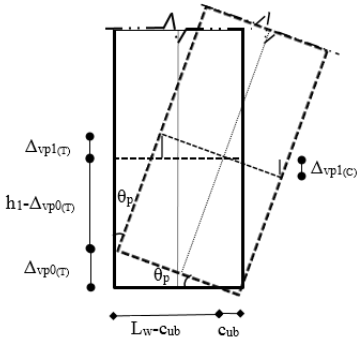

b) Plastic deformation of a wall

Figure 13: Elastic and plastic deformation of a wall.

Note that in deriving these equations the NA depth in the elastic phase is assumed at mid-length of the wall. In reality, during elastic response the NA is located closer to the centre than at ultimate stage but its exact location in the compression half changes with wall characteristics. Consequently, this assumption will slightly underestimate the upward movement of the wall's tensile edge (and the resulting out-of-plane shear displacement of the floor connected to it) and overestimate, by an equal amount, the downward movement of the wall's compression edge (and the shear displacement of the connected floor). For walls with equal floor spans beyond the two edges, this means there will be no change to the wall moment. This logic is validated by the derivations and case study presented later. For walls with different floor spans beyond the two edges, the error induced will be insignificant as the wall's elastic deformation accounts for only a small proportion of the total floor displacement. Hence, for simplicity this assumption is justified as it does not compromise the final results.

It is important to highlight that storey rotations (and consequently the wall edges displacements) during the elastic response shown in Figure 13(a) are controlled by the cumulative summation of curvatures below the given storey level, while the plastic displacements of the wall edges at a specified height from the base (or at a given storey level) is solely controlled by the base plastic hinge rotation.

In the procedure followed herein, the wall edge vertical plastic displacements at a storey level (denoted as Δ_{vpi}) are estimated based on the value of the base plastic rotation (θ_p), the neutral axis depth at the ultimate section response (c_{ub}) and the height of the storey (h_i). The challenge is to find the plastic rotation at the wall base. The appropriate value of the base plastic rotation highly depends on the assumed/selected plastic hinge length and the ultimate curvature of the wall section. In this study, the experimentally validated plastic hinge length (equal to one-third of the wall length) recommended by Thomsen and Wallace [38] is adopted. They demonstrated that plastic hinge length between 0.33Lw and 0.5Lw was found to produce a very good agreement with the measured strain profiles, and for rectangular walls better agreement was obtained with 0.33Lw. The plastic hinge length of 0.33Lw adopted here has also been validated against experimental data from building tests [18].

Plastic rotation of a wall at the base section and corresponding deformation of the wall are shown in Figure 13(b). Due to the plastic rotation of the wall, the vertical displacements of the two wall edges are estimated using the following steps:

- Calculate the effective yield curvature ϕ_{yeff} at the base section using Equation (11) or Equation (13).
- Estimate the ultimate curvature ϕ_u from the moment-curvature section analysis.

  Alternatively, Equation (16) proposed in literature [37] can be used to estimate the ultimate curvature without conducting a moment curvature analysis.

$$\phi_u L_w = 0.8 C_L(\varepsilon_{su})(1 - 2.4\frac{P}{P_o})(1 - 1.5\frac{f_y}{f_c}\rho_{sh})(\frac{M/V}{L_w})^{0.29} \quad (16)$$

  where C_L is a coefficient that takes into account the effect of loading regime with the proposed values of 0.75 and 1.0 in case of cyclic and monotonic loadings, respectively, ε_{su} is the ultimate strain capacity of the reinforcing steel (strain at rupture), P_o is the nominal axial load capacity at zero eccentricity, P is the applied axial load, f_y is the yield strength of longitudinal reinforcement in the boundary region, f_c is the specified compressive strength of concrete, ρ_{sh} is the ratio of web horizontal reinforcement to vertical cross section, M/V is the applied moment to applied shear force ratio, and L_w is the wall length.
- Use plastic hinge length $l_p = 0.33L_w$ to estimate the plastic hinge rotation $\theta_p = l_p (\phi_u - \phi_{yeff})$
- Determine the neutral axis depth (C_{ub}) at the maximum flexural strength from moment-curvature analysis or by using the charts in Figure 12(b).
- Calculate the wall edge vertical displacements at different storey levels due to plastic rotation as:

$$\Delta_{vp0(T)} = (L_w - c_{ub}) \times \theta_p \,, \Delta_{vp0(C)} = c_{ub} \times \theta_p \quad \text{at the base} \quad (17)$$

$$\Delta_{vpi(T)} = \Delta_{vp0(T)} - h_i \times (1 - cos\theta_p) \quad \text{at storey i} \quad (18)$$

$$\Delta_{vpi(C)} = \Delta_{vp0(C)} + h_i \times (1 - cos\theta_p) \quad \text{at storey i} \quad (19)$$

where h_i is the height of the storey *i* from the base, and $\Delta_{vpi(T)}$ and $\Delta_{vpi(C)}$ are respectively the upward and downward plastic displacements of the tension and compression edges at the storey level *i*.

The total upward or downward displacement of a wall edge is equal to the sum of the elastic and plastic displacements calculated above.

FLOOR SLABS CONTRIBUTION

To quantify the contribution of floor slabs to the lateral response of multi-storey structural wall buildings, two-way floor slabs in each floor are modelled as a grid of orthogonal equivalent elastic beams intersecting at the edges of walls present in that floor plan. In such buildings, slabs are subjected to out-of-plane actions due to upward/downward movements of their boundaries connected to the structural walls. Hence, the floor slabs bend not only like beams in orthogonal directions, but they are also subjected to torsional warping, which can be non-trivial in irregular floor plans. However, torsional stiffness of the slabs is ignored here to derive a simple hand calculation method.

Figure 14 shows a representative floor plan with structural walls as lateral load resisting elements. Here, two walls resist the lateral forces in each direction, but mechanisms and system behaviour related to only one wall along the Y-axis are discussed here for brevity; the process explained herein can be readily followed to deduce the behaviour of the remaining three walls. Altogether for this floor, there will be beams along four gridlines each in the X and Y directions, which intersect at the edges of the walls. Each wall will interact with all beams spanning through the two edges of the wall in either directions. For example, the shaded cruciform area in the figure indicates the portion of the slab interacting with the Y-direction wall in gridline B. The hatched portion indicates the slab strip acting as the Y-direction beam restrained vertically at the far ends by gravity columns and connected to the wall in the central region. This beam will be forced to move up/down and rotate together with the wall edge when the wall deforms in-plane. On the other hand, the two solid strips orthogonal to the wall axis represent the X-direction beams which are supported at the far ends by the gravity columns on either side of the wall. When the wall deforms in-plane, these beams will be forced to move vertically together with the wall edges.

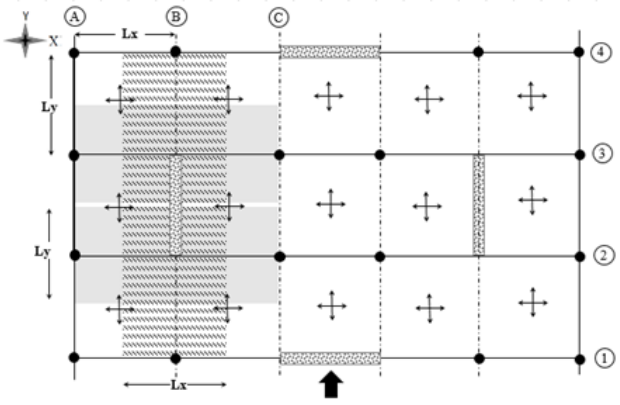

Figure 14: Equivalent slab lengths and widths in X and Y directions in a typical floor plan.

The equivalent slab widths represented by the X and Y direction beams are equal to the bay length in the orthogonal direction. For example, the beam spanning along the wall axis has length L_Y (i.e. bay span in Y-direction) and represents slab width equal to L_X (bay length in X-direction); and vice versa. As the purpose of representing strips of floor slabs as equivalent beams in this study is to find the best estimate of shear force transferred as axial forces to the gravity columns via out-of-plane bending deformation of the slabs, the equivalent width is assumed to be the width of the tributary area; i.e. equal to the bay length (covering half of the bay on each side). This makes it easy to replace them with an equivalent beam type element. However, it is obvious that the deformation of slabs out of their horizontal plane also induces some additional axial forces in the corner columns. In this study, the contribution of axial force in the corner columns (which will be small in comparison to the six columns that are included in the shaded area) is neglected. As will be revealed later, results of the hand calculation method confirm that this is a reasonable assumption.

As the flexural stiffness of the gravity columns supporting the beams at the end is negligible compared to the flexural stiffness of the slabs, the wall-floor-column sub-assemblage can be reasonably represented by a beam with a pin at the far end from the wall. The wall ends of the equivalent beams follow the deformation of the wall edge they are connected to. Hence, the enforced boundary conditions stem from the vertical displacement of the wall edges as well as the sectional rotation of the wall at each floor level. Thus, these vertical and rotational deformations are prescribed as boundary conditions for the equivalent beams at their connections to the wall.

MAXIMUM MOMENT CAPACITY OF THE SYSTEM

Any in-plane deformation of shear walls will force the floor slabs to deform and trigger vertical reactions at their end supports, which will induce axial forces in the walls and gravity columns. The additional moment capacity induced in the building due to these column axial forces at the ultimate limit state can be estimated using the formulation derived below.

First, the wall edges' vertical displacements at each storey level need to be calculated at the effective yield and ultimate limit states. For this, wall rotations along the wall height at these two limit states are required.

The rotation profile at yielding limit state can be calculated using Equation (5) by substituting ϕ_{yeff} for ϕ_{base} and replacing z with the variable h_i. Thus, the rotation of each storey at the effective yielding base curvature can be obtained using Equation (20).

$$\theta_{yi}(z = h_i) = \left(\frac{\phi_{yeff}}{8H^3} h_i^4 - \frac{3\phi_{yeff}}{4H} h_i^2 + \phi_{yeff} h_i\right) \quad (20)$$

Similarly, the maximum plastic rotation of the wall can be obtained by assuming equal plastic curvature (i.e. difference between the ultimate and yielding curvatures) distributed across the plastic hinge length at the base of the wall. This yields Equation (18), which is employed here to estimate the plastic hinge rotation.

$$\theta_p = (\phi_u - \phi_{yeff}) \times l_p \quad (21)$$

At the ultimate limit state, the total rotation of the wall section at each storey is the summation of the elastic rotation at that storey given by Equation (20) and the plastic rotation at the wall base given by Equation (21). Note that using the plastic rotation capacity (rather than plastic rotation demand at the design level of drift) ensures that the wall behaves in the intended ductile mode all the way until its ultimate limit state. Thus derived system overstrength factor may be slightly conservative at design demand, but this will reassure that the system performance will not be catastrophic even at shakings exceeding the design level. Similarly, the vertical movements of the wall edges can also be obtained by summing the vertical movements due to elastic and plastic rotations (as explained in the previous section while discussing Figure 12).

$$\delta_{ti} = \Delta_{vei(T)} + \Delta_{vpi(T)} \qquad \delta_{ci} = \Delta_{vei(C)} + \Delta_{vpi(C)} \quad (22)$$

In Equation (22), δ_{ti} and δ_{ci} are the vertical displacements of respectively the tension (upward) and compression (downward) edges at storey level *i* due to the total sectional rotation of the wall at the ultimate limit state. To calculate these ultimate state vertical displacements of the wall edges in each floor due to an arbitrary lateral force, Equation (20) and Equation (22) should be used along with the derivation of elastic and plastic vertical displacements presented in the previous section (see Figure 13 and Equations (18) and (19)). This results in the following

equations for wall edges vertical displacements in tension and compression sides.

$$\delta_{ti} = \left(\frac{\phi_{eff}}{8H^3}h_i^4 - \frac{3\phi_{eff}}{4H}h_i^2 + \phi_{yeff}h_i\right) \times \left(\frac{L_w}{2}\right) + (L_w - c_{ub}) \times \theta_p - h_i(1 - cos\theta_p) \quad (23)$$

$$\delta_{ci} = \left(\frac{\phi_{yeff}}{8H^3}h_i^4 - \frac{3\phi_{yeff}}{4H}h_i^2 + \phi_{yeff}h_i\right) \times \left(\frac{L_w}{2}\right) + (c_{ub}) \times \theta_p + (1 - cos\theta_p) \quad (24)$$

These vertical displacements along with the total sectional rotation ($\theta_i = \theta_{yi} + \theta_p$) are enforced as the boundary conditions to the equivalent beams representing the adjacent floor slabs. Figure 15 illustrates the application of these boundary conditions on the equivalent beams in Y and X directions. The far support of the beams at the gravity columns are treated as pins, which imply that any minor elastic axial displacement due to the axial force induced in the gravity columns is overlooked. Also, assuming the out-of-plane displacements are small in comparison to the floor dimensions (i.e. small-displacement theory), any minor membrane force induced in the floor slab and consequent shear force induced in the columns due to the transverse deformation (and catenary action) of the floor are ignored.

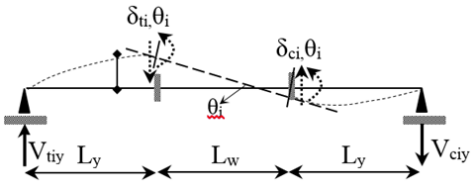

Equivalent beam in Y direction (storey i)

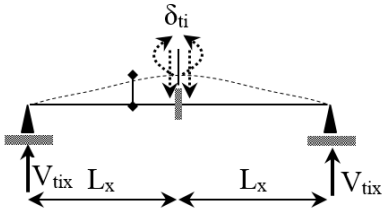

equivalent beam in X direction (Tension side)

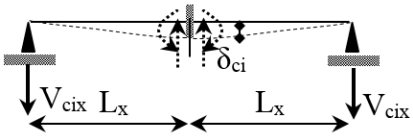

equivalent beam in X direction (Compression side)

Figure 15: Equivalent beams in X and Y directions and boundary conditions enforced due to deformation compatibility.

For the beam in Y-direction, the vertical reactions at the two supports are of opposite nature; the upward reaction in the left support (inducing tension in the column) is denoted as V_{tiy} and the downward reaction in the right support (inducing compression in the column) is denoted as V_{ciy}. These reactions, which are equal to the column axial forces, can be calculated as:

$$V_{tiy} = \frac{3EI_{eff} \times \delta_{ti}}{L_y^3} + \frac{3EI_{eff} \times \theta_{ti}}{L_y^2} \quad (25)$$

$$V_{ciy} = \frac{3EI_{eff} \times \delta_{ci}}{L_y^3} + \frac{3EI_{eff} \times \theta_{ti}}{L_y^2} \quad (26)$$

where, δ_{ti} and δ_{ci} are defined in Equation (22), θ_{ti} is the total rotation calculated as $\theta_{yi}+\theta_p$, E is the elastic modulus of concrete and I_{eff} is the moment of inertia of the effective section of the beam including the effect of cracking. Acceptable values of effective section inertia as a fraction of gross section inertia are recommended in concrete codes for floor slabs and/or beams, which can be used in this calculation.

In contrast, for the two beams spanning along X-direction, the reactions at both supports are of the same nature. As can be seen in Figure 15, the X-beam spanning across the tension edge will develop upward reaction at both supports (inducing axial tension on the columns) and the beam spanning across the compression edge will develop downward support reactions (inducing axial compression on the columns). Note that the twisting (i.e. transverse bending) of the X-direction beams induced by the in-plane deformation of the wall is not accounted for in this derivation. The reactions at the two supports will be equal if the spans in the two sides of the wall are equal (which is true for the case considered here). These reactions can be calculated as:

$$V_{tix} = \frac{3EI_{eff} \times \delta_{ti}}{L_x^3} \quad and \quad V_{cix} = \frac{3EI_{eff} \times \delta_{ci}}{L_x^3} \quad (27)$$

Note that the effective section inertia of the X-direction beams can be fairly assumed to be equal to Y-direction beams in two-way flat slabs, but this is not true when profiled precast flooring units are used. For example, the effective section inertia of double tee or hollow core in the transverse direction will be significantly less than that in the longitudinal direction because only the thin flanges participate in resisting floor bending in the transverse direction. In such cases, effective section properties shall be calculated separately for the two directions.

Figure 16 illustrates the deformed shape of a structural wall cross section in a typical floor of a multi-storey structural wall building and a schematic spatial representation of the induced actions in the surrounding gravity columns. The axial forces induced in the gravity columns generate an extra moment in each storey, which is surplus to the sectional moment capacity of the structural walls. This additional moment capacity due to system interaction can be estimated in each storey by multiplying the axial forces in the columns by their distance from the centre of the wall section.

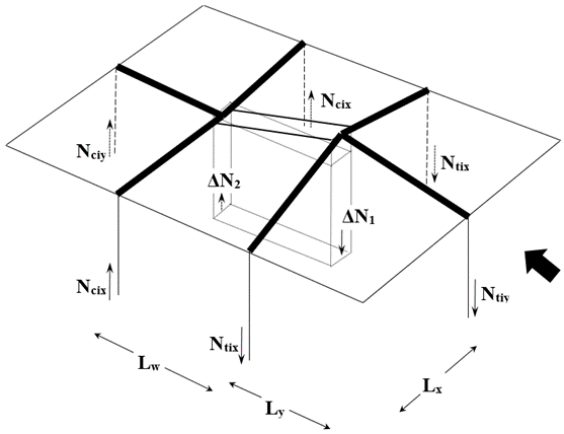

Figure 16: Induced axial forces in gravity columns/walls due to structural wall sectional deformation compatibility.

The steps followed herein to estimate the additional axial forces induced in gravity columns due to their interactions with the wall deformation via floor slabs in each storey, and to quantify their contribution to the storey level moment and shear demands are outlined below.

- Calculate the effective widths of the slabs in X and Y directions; i.e. L_x and L_y respectively.

- Calculate the shear forces induced in the equivalent beam elements at storey *i* in the X direction; i.e. V_{tix} and V_{cix} using Equation (27).
- Calculate the shear forces induced in the equivalent beam element at storey *i* in the Y direction; i.e. V_{tiy} and V_{ciy} using Equations (25) and (26).
- Add the shear forces from all higher floors to obtain the additional column axial forces due to wall-floor-column interaction.

$$N_{tjy} = \sum_{i=j}^{n} V_{tiy} \qquad N_{cjy} = \sum_{i=j}^{n} V_{ciy} \tag{28}$$

$$N_{tjx} = \sum_{i=j}^{n} V_{tix} \qquad N_{cjx} = \sum_{i=j}^{n} V_{cix} \tag{29}$$

- Calculate the additional system moment induced in the storey due to the wall-floor-gravity frame interaction by adding the moments (about the centre of the wall) of the additional axial forces induced in all columns in that storey.

$$M_{int,i} = \left(N_{tiy} + N_{ciy}\right)\left(L_y + \frac{L_w}{2}\right) + 2(N_{tix} + N_{cix})\left(\frac{L_w}{2}\right) \tag{30}$$

  Note that if the bay lengths are not equal, the lever arms of the tensile and compressive forces could be different and the storey moment calculation takes a different form. Moreover, when the whole floor including multiple walls in a symmetric floor plan is considered, the moments of the column axial forces could be taken about geometric centre of the floor (rather than the centre of a particular wall).
- Calculate the additional storey shear demand introduced to the structural walls due to axial forces induced in the columns.

$$V_{int,i} = \frac{M_{int,i}}{h_i} \tag{31}$$

The proposed procedure enables accounting for the differences in the boundary conditions (i.e. different wall rotations and movements of the wall edges) at different storey levels. The actions induced in the tension and compression sides of the structural walls are estimated separately. Applying Equation (30) to the bottom storey and substituting for the column axial forces from Equations (25)-(29), the moment resisted by the system interaction at the base can be written as below.

$$M_{int,base} = \sum_{i=1}^{n}\left(\frac{3EI_{eff}\delta_{ti}}{L_y^3} + \frac{3EI_{eff}\theta_i}{L_y^2}\right)(L_y + L_w/2) + \sum_{i=1}^{n}\left(\frac{3EI_{eff}\delta_{ti}}{L_x^3}\right)\left(\frac{L_w}{2}\right) \times 2 + \sum_{i=1}^{n}\left(\frac{3EI_{eff}\delta_{ci}}{L_y^3} + \frac{3EI_{eff}\theta_i}{L_y^2}\right)(L_y + L_w/2) + \sum_{i=1}^{n}\left(\frac{3EI_{eff}\delta_{ci}}{L_x^3}\right)\left(\frac{L_w}{2}\right) \times 2 \tag{32}$$

This additional moment or resistance of the system calculated at the ultimate limit state together with the moment capacity of the wall gives the moment overstrength of shear wall building system, which can be normalized with respect to the nominal flexural strength of the wall base section to evaluate the system overstrength factor.

$$\Omega_s = \frac{M_{wall-nominal} + M_{wall-hardening} + M_{int,base}}{M_{wall-nominal}} = 1 + \frac{M_{wall-hardening}}{M_{wall-nominal}} + \frac{M_{int,base}}{M_{wall-nominal}} = 1.15 + \frac{M_{int,base}}{M_{wall-nominal}} \tag{33}$$

The hardening component of the overstrength is required only in the hand calculation method. In finite element analysis, the effect of hardening can be automatically accounted for in the predicted nominal capacity by employing material laws including strain hardening of rebar and confinement effect of concrete. For consistent comparison, only the strain-hardening component of the material overstrength (assumed as 1.15) is used in deriving the hand calculation method for flexural strength of rectangular walls. This is in line with the post-yielding moment capacity suggested by section analysis using material models accounting for the strain hardening of reinforcing bars and confinement of concrete. This procedure implies a consistent comparison between the system overstrength obtained from the finite element analysis and from the simplified method.

The system overstrength (including the additional moment capacity due to the interaction between the walls and the gravity columns through the floor slab) could be critical when capacity design principle is to be applied to avoid shear failure of the structural walls. Hence, this study applies the above-explained procedure to typical configurations of structural wall buildings to obtain a reliable value of the system overstrength for capacity design of multi-storey RC structural wall buildings.

SCRUTINIZING THE HAND CALCULATION APPROACH

The proposed simplified hand calculation method using the derived formulations is applied to a building prototype with slab length equal to 6 m in both directions and an effective flexural stiffness equal to 25% of gross section stiffness (i.e. $EI_{eff} = 0.25EI_g$). Sectional properties of the wall are the same as those considered in the previous section; i.e. as presented in Figure 2. To distinguish this case from the status quo approach of no wall-floor interaction, it is identified as Case 2.

Estimation of the Wall Edges Vertical Displacements and Sectional Rotation

For the designed wall section in the prototype building, the effective yield curvature, the yield moment and the effective flexural stiffness are obtained from section analysis as ($\phi_{yb} = \phi_{yeff} = 0.6646$/km, $M_{nb} = 37905$kN.m, $I_{eff} = 1.901$m^4, $I_{eff}/I_g = 0.265$) respectively. Using these values, the curvatures and the elastic rotations of the wall in each story level are calculated by employing the proposed method. The calculated values are listed in Table 3.

As can be observed in the table, the vertical displacements of the wall edges increase with the height of the floor from the base. For example, the total vertical displacement in the tension side is equal to 116.9 mm at roof level and 108.3 mm in the first storey. Nevertheless, this difference is small and it would be acceptable to ignore the second order effects in calculating the wall edge displacement profile across the wall height. Similarly, it is also evident from the values in Table 3 that the wall edge displacements (particularly the tension edge) increase drastically in the nonlinear stage. For example, the elastic and plastic vertical displacements of the tension edge at the roof level are equal to 19.14 mm and 97.73 mm respectively. Hence, it is critical to assess the effect of system interaction at the ultimate limit state in design or assessment of structural wall buildings.

Calculation of Induced Actions

In this section, based on the estimated values of the vertical displacements of the wall edges in tension and compression sides as well as the sectional rotation (Table 3), the additional design actions induced in different storeys are calculated using the proposed method. Table 3 presents the values of the axial forces induced in the columns and their corresponding moments at each storey level. As can be seen in this table, the extra base moment capacity induced in the bottom floor due to system interaction is equal to 16981.35 kNm, which is about 45% of the nominal yielding moment capacity of the wall section (i.e. 37905 kNm). Combining with the 15% overstrength due to strain hardening, this results in a system overstrength equal to 1.6 for this building configuration.

Table 3: Elastic and plastic vertical displacements of wall edges for Case 2.

Storey level	0 (Base)	1	2	3	4	5	6	7	8 (Roof)
Curvature(ϕ_i) (1/km)	0.6646	0.6651	0.6674	0.6816	0.7054	0.7448	0.8037	0.8859	0.9954
θ_{yi} (rad)	0	0.0019	0.0035	0.0046	0.0054	0.0060	0.0063	0.0064	0.0064
Δ_{vei}(T) (mm)	0	5.78	10.40	13.88	16.35	17.92	18.77	19.10	19.14
Δ_{vei}(C) (mm)	0	5.78	10.40	13.88	16.35	17.92	18.77	19.10	19.14
θ_p(rad)	0.0207	-	-	-	-	-	-	-	-
Δ_{vpi} (T) (mm)(upward)	103.20	102.52	101.84	101.15	100.50	99.78	99.10	98.42	97.73
Δ_{vpi}(C) (mm)(downward)	-	21.53	22.21	22.89	23.57	24.26	24.94	25.63	26.31
$\delta_{ti} = \Delta_{vei}(T) + \Delta_{vpi}(T)$ (mm)(upward)	103.2	108.30	112.24	115.03	116.85	117.70	117.87	117.52	116.87
$\delta_{ci} = \Delta_{vei}(C) + \Delta_{vpi}(C)$ (mm)(downward)	-	27.31	32.61	36.79	39.92	42.18	43.71	44.73	45.45
$\theta_{ti} = \theta_{yi} + \theta_p$ (rad)	0.0207	0.0226	0.0242	0.0253	0.0261	0.0266	0.0269	0.0270	0.0270

Table 4: Extra moment due to the induced actions in gravity columns in each storey for Case 2.

Storey level	θ_{ti} (rad)	N_{tiy} (kN)	N_{ciy} (kN)	N_{tix} (kN)	N_{cix} (kN)	$M_{sys,i}$ (System moment) (kN.m)	Ω_{si}
8	0.0270	-116.33	86.57	-48.70	18.94	2232.0	
7	0.0270	-232.89	172.80	-97.66	37.57	4462.61	
6	0.0269	-349.33	258.34	-146.77	55.78	6684.30	
5	0.0266	-464.99	342.53	-195.82	73.36	8882.73	
4	0.0261	-578.97	424.48	-244.49	89.99	11037.93	
3	0.0253	-690.16	503.05	-292.42	105.32	13125.32	
2	0.0241	-797.27	576.98	-339.18	118.90	15116.71	
1(Total)	0.0226	-898.90	644.86	-384.31	130.28	16981.35	1.60

From the above example, it is obvious that the system interaction between the walls, floor slabs and gravity frames can significantly increase the moment capacity of multi-storey structural wall buildings. Such flexural overstrength can alter the strength hierarchy of different failure modes and render the building to fail in an undesirable and brittle mode. Needless to mention, this additional flexural overstrength due to system interaction must be properly accounted for in designing RC wall buildings.

Effect of Floor Characteristics

To better understand the three-dimensional spatial effects of slabs on the system behaviour of multi-storey shear wall buildings and to recommend reliable system overstrength factors for design, five variants of the prototype building are analysed hereafter. As is apparent from the derivations in the previous sections, the parameters governing the induced extra moment are the wall edge displacements and the flexural stiffness of the equivalent beams representing the slab spanning in the two directions. The wall edge displacements are controlled by the lateral forces and the wall characteristics, so they do not depend on the building configuration. Nevertheless, the flexural stiffness of the equivalent beams are controlled by the effective section stiffness of the floor slabs and the beam span (i.e. bay length) in the two directions. Hence, these two key parameters (slab stiffness and the bay lengths) are altered in these five cases to assess their effects on the system overstrength.

The flexural stiffness and geometrical dimensions of the floor slab used in these five cases are listed in Table 5. Typical floor plan and geometry of the prototype building have already been defined in the previous section (see Figure 2 and Table 1). In all five cases, the structural wall properties remain the same while the bay length in the two directions and/or the flexural stiffness of the floor slab are varied. With zero floor stiffness, Case 1 represents an uncoupled system where the effect of the system interaction is fully overlooked. To trigger the interaction between the wall and gravity columns through the floor slabs, non-zero floor stiffness are assigned in other 4 cases. Floor stiffness equal to 25% of the gross section stiffness is assigned in Cases 2-4 and Case 5 is assigned floor slabs with 50% of the gross stiffness. Note that this range of stiffness is chosen to include the effective section inertia used in design, which is typically 0.3-0.4 of the gross moment of inertia (I_g) for beams and ~0.25I_g for slabs. Case 2 is the same as that analysed in the previous section (see Tables 3 and 4). Cases 3 and 4 are selected to represent the effect of change in (bay) length of slabs in X and Y directions, respectively. Similarly, Cases 1, 2 and 5 will provide the effect of the flexural out-of-plane stiffness of the slabs.

Table 5: Variables for different case studies.

Case	Floor slab flexural stiffness	L_x (m)	L_y (m)
1	0	6	6
2	0.25EI_g	6	6
3	0.25EI_g	6	8
4	0.25EI_g	8	6
5	0.50EI_g	6	6

Finite Element Modelling

To scrutinize the application of the proposed hand calculation method, the system overstrength factors for these five cases are calculated by following the simplified procedure developed in the previous section. Moreover, finite element analyses are also conducted to generate the pushover response of these five cases, which help in verifying the reliability of the proposed hand calculation method. Three-dimensional nonlinear finite element models are developed for the prototype building using SAP2000 [39], and floor stiffness and lengths are assigned as listed in Table 5 to obtain their pushover capacity curves. The seismic masses at all floors are assigned as distributed mass on walls. A rigid diaphragm action is enforced by slaving the translational degrees of freedom at each floor level. The foundation of the building is assumed as rigid, and P-delta effects are taken into account.

Several micro and macro modelling techniques are available to model and analyse RC walls [40,41]. Novel quadrilateral elements with superior computational efficiency and accuracy have also been proposed in literature [42-44]. Although nonlinear response and different failure modes of isolated walls can be convincingly predicted using existing techniques [45], many challenging issues still remain in modelling nonlinear behaviour of shear walls in multi-storey buildings [46]. In this study, nonlinear shell elements that have been validated in predicting in-plane behaviour of RC structural walls [47] are used to model the rectangular walls. Confined and unconfined concretes are modelled differently using stress-strain relationships (shown in Figure 17b) proposed by Mander et al. [35], and the tensile strength of concrete is neglected. The stress-strain relationship used for the steel reinforcement is shown in Figure 17(a). Shear behaviour is modelled using the automated inelastic shear layer in SAP2000 [39] for nonlinear shell elements.

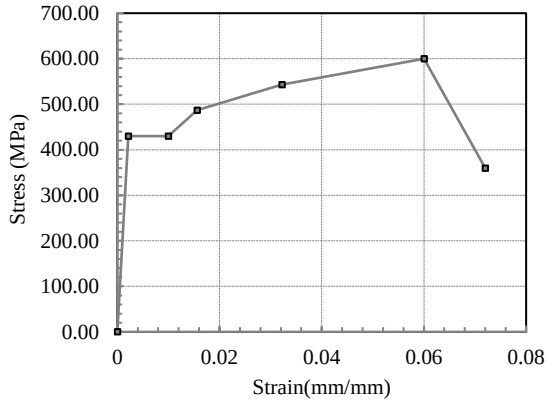

(a)

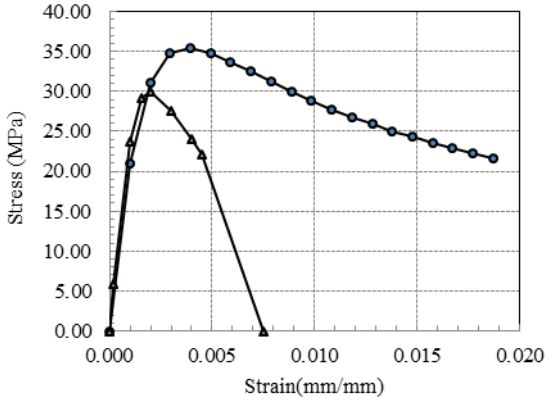

(b)

Figure 17: Material stress-strain backbone curves; a) Reinforcement b) Concrete.

Slabs are modelled using elastic shell elements with effective flexural stiffness values as per the Case being considered, and the shear stiffness of the slabs is taken as half of the gross shear stiffness; i.e. $GA = 0.5GA_g$, where the shear modulus (G) is calculated using a Poisson's ratio $\nu = 0.2$. All slabs are assigned a specified concrete strength of $f'_c = 30$ MPa.

The gravity columns are modelled as elastic beam elements with very low flexural stiffness. Elastic properties of the columns are evaluated using the cross-section dimensions, and the following stiffness modification factors are used for the columns in flexure and shear; $EI_{eff} = 0.01EI_g$ (flexural), $GA = 1.0GA_g$ (shear). Figure 18(a) shows the first elastic mode shape of the whole structure with a period equal to 0.80 sec. As an example of the predicted response, Figure 18(b) depicts the von Mises stress of concrete layers for Case 1 at the last loading step before the peak strength of system starts decreasing.

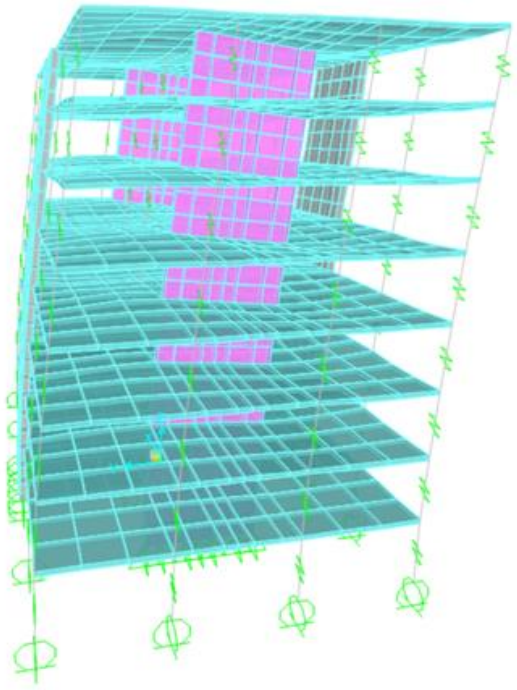

(a)

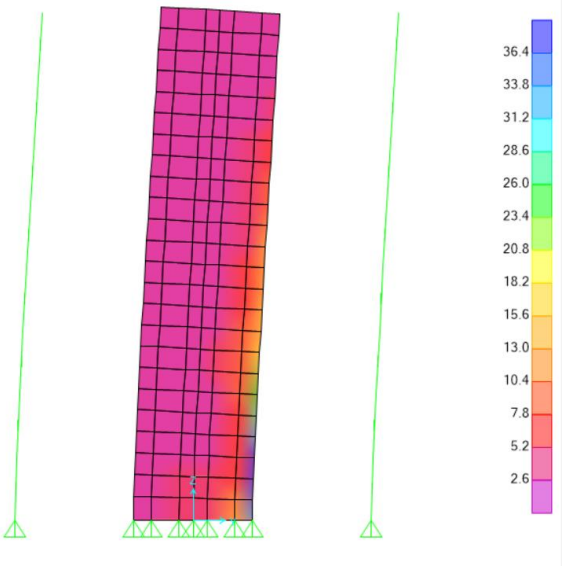

(b)

Figure 18: a) First elastic mode of finite element model; b) The von Mises stress of concrete layer at the peak strength (for Case 1).

Analysis Method and Results

In this study, pushover analyses are conducted by primarily applying lateral forces proportional to the shape of the first mode to the selected prototype building. Although the logical distribution of lateral load pattern in pushover analysis should ideally be updated regularly due to gradual reduction of the system stiffness during the analysis (due to cracking, yielding and force redistribution), the initially assigned load pattern is retained for the whole analysis in this study as per FEMA-450 [27] guidelines. All analyses are performed with a gravity load of P=1.0D+0.25L. The analytically predicted pushover curves are then idealized according to FEMA-695 [48] approach where/if needed.

The results of displacement controlled pushover analysis for all cases are compared in Table 6, and pushover curves of three cases with the same dimension but different slab stiffness are plotted in Figure 19. To find the effective period of the building, the estimated capacity curve can be idealized to obtain an equivalent single degree of freedom system. Detailed description of converting the multiple degrees of freedom capacity curve to the equivalent single degree of freedom capacity curve can be found in ATC-40 [49]. It is evident from Table 6 that Cases 2 to 5 develop considerable overstrength due to contribution of floor slabs in the system response.

Table 6: Results of pushover analysis.

Case	Base flexural yielding* (M_{by}, θ_y)	Maximum base moment* (M_u, θ_u)	Ω_s**
1	(33.70,0.00123)	(42.61,0.0191)	1.26
2	(37.35,0.00123)	(64.36,0.0191)	1.72
3	(37.04,0.00123)	(62.95,0.0192)	1.70
4	(36.93,0.00122)	(62.24,0.0192)	1.68
5	(40.45,0.00122)	(82.54,0.0186)	2.04

*Units: MN.m and rad, excluding the p-delta effect
** normalized with respect to M_{by}

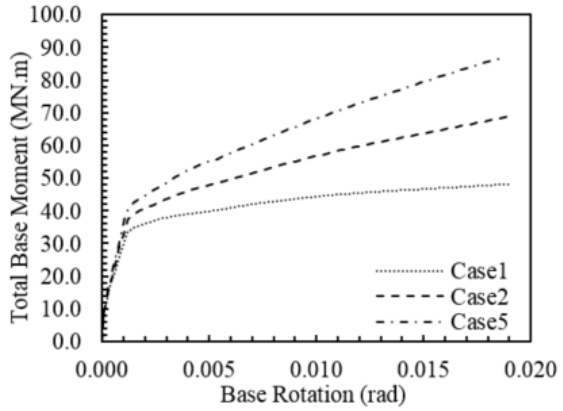

Figure 19: Results of pushover analysis for three cases (including p-delta effect).

Comparing the pushover curves in Figure 19 demonstrates that the slab out-of-plane stiffness starts contributing significantly to the overall strength of the system when the structural walls gradually enter the inelastic range after reinforcement yielding in the wall boundary elements. The significant yield point is defined here as the instant when reinforcement in the boundary element yield in tension or when the element representing the boundary zone in the numerical model yields. In other words, the stress of boundary zone reinforcing bars, smeared into the mesh of the boundary elements, is tracked in each step of the analysis and once all reinforcing bars inside the boundary mesh yield, the base yield moment (M_{by}) and the yield rotation are recorded. The base rotation is determined by dividing the sum of the vertical displacements of the two wall edges (measured within the bottommost $0.33L_w$) by the wall length.

From the five cases investigated, two (Case 1 and Case 2) are selected here for detail comparison of responses at yielding and at specific drift levels. At the base rotation of 0.0191 rad, the ratio of the base moment in Case 2 (64.36 MN.m) to that in Case 1 (42.61 MN.m) is equal to 1.51. The contribution of system interaction on the base moment resistance at yielding point is approximately 11% larger in Case 2 than in Case 1 with no interaction. Case 1 reaches the maximum system overstrength equal to 1.26 at the base rotation of 0.0191 rad. However, the maximum overstrength in Case 2 is found to be 1.72 at the same base rotation. While the overstrength of Case 1 is attributed mainly to strain hardening and confinement of concrete in the critical section, Case 2 benefits much more from the contribution of wall-slab-column interaction in resisting the lateral forces.

The remaining cases were also analysed to verify the reliability of the simplified hand calculation method. The numerical analyses results also address the importance of bay length as well as the flexural stiffness of slabs on the system overstrength factor. The calculated and analytically predicted values of system overstrength and the associated error for all five cases are presented in Table 7. In order to compare the results of hand calculation method with the finite element method, the maximum base moment capacity obtained by the finite element analysis is normalized to the nominal flexural strength of walls.

Table 7: Comparison between the proposed hand calculation method and finite element analysis results.

Case	$\Omega^*_{\text{Finite element}}$	Ω^*_{simple}	Error
1	1.12	1.15	2.6%
2	1.70	1.60	6.25%
3	1.66	1.46	13.7%
4	1.64	1.55	5.81%
5	2.18	2.05	6.34%

*Normalized with respect to M_n

Table 7 demonstrates that in the five case studies examined here, the overall error in estimation of moment overstrength is on average 7 percent. In the cases investigated herein, the system overstrength due to interaction between the walls, slabs and gravity columns vary between 1.70 and 2.18. It is also evident that doubling the out-of-plane stiffness of slabs increase the system overstrength by 28%. Changing the bay length from 6 m to 8 m in either directions is found to reduce the system overstrength by only about 3%. It seems that the value of Ω_s mostly depends on the flexural stiffness of slabs to a large extent and bay length to a smaller extent.

The following three assumptions may slightly alter the predicted overstrength values. First, the simplified method overlooks the presence of corner columns and the boundary conditions imposed by them to the slabs. Second, the effective width of the slabs is assumed to be equal to the bay length in calculating the out-of-plane stiffness of the equivalent beams representing the floor slab. Third, any variation in the axial force on the structural wall itself due to the wall floor interaction is neglected in the hand calculation method. These assumptions are made for simplicity/brevity and the sensitivity of the predicted overstrength values to these assumptions require further investigation. Moreover, experimental results on RC wall building systems are currently scarce [18], and future studies should aim to conduct more system level experimental tests to validate (and fine-tune if needed) the proposed method.

CONCLUSIONS

The effect of wall-slab-gravity system interaction on the overall behaviour of RC structural wall buildings is explored in this paper. Through a simplified analytical and numerical investigation, it is confirmed that the out-of-plane stiffness of floor slabs can induce significant additional axial forces in gravity columns and this interaction can increase the system moment capacity and the corresponding overstrength of multi-storey structural wall buildings. In capacity design philosophy, this overstrength may affect the strength hierarchy of different failure modes of the structural walls mainly due to additional shear force demand induced in different storeys of the structural walls. This system interaction effect requires additional allowance in base shear demand calculation and shear force envelope proposed for the structural walls.

Based on theoretical elastic and plastic analyses enforcing compatibility and equilibrium between the interacting components (structural walls, floor slabs and gravity columns), generalised equations to express the lateral displacement and rotation profiles as a function of the yielding curvature of the wall base section. Equations are also developed to relate the roof displacement of multi-storey wall buildings to the base curvature in the elastic stage and to the plastic rotation in the nonlinear range. These relationships enable estimation of engineering demand parameters (such as inter-storey drift) of wall buildings without conducting complex numerical modelling and analysis.

Moreover, a generalized and simple method is proposed which can enable hand calculation of the additional axial forces induced in gravity columns of structural wall buildings and estimation of the resulting system overstrength without using a rigorous finite element analysis.

While to achieve robust values for the system overstrength, structural wall buildings with a wide range of arrangements of structural walls and floor slabs should be investigated, based on the limited number of cases investigated herein a system over strength factor of 1.7 appears reasonable as an interim guidance to account for system interaction effects in ductile multi-storey RC structural wall buildings typical of NZ design.

REFERENCES

1 Kam WY, Pampanin S and Elwood K (2011). “Seismic performance of reinforced concrete buildings in the 22 February Christchurch (Lyttelton) earthquake”. *Bulletin of the New Zealand Society for Earthquake Engineering*, **44**(4): 239-278. https://doi.org/10.5459/bnzsee.44.4.239-278

2 Telleen K, Maffei J, Willford M, Aviram A, Huang Y, Kelly D and Bonelli P (2012). “Lessons for concrete wall design from the 2010 Maule Chile earthquake”. *Proceedings of the International Symposium on Engineering Lessons Learned from the 2011, Great East Japan Earthquake*, March 1-4, Tokyo, Japan.

3 Wallace JW, Massone LM, Bonelli P, Dragovich J, Lagos R, Lüders C and Moehle J (2012). “Damage and implications for seismic design of RC structural wall buildings”. *Earthquake Spectra*, **28**(SUPPL.1): S281-S299. https://doi.org/10.1193/1.4000047

4 Sritharan S, Beyer K, Henry RS, Chai Y, Kowalsky M and Bull D (2014). “Understanding poor seismic performance of concrete walls and design implications”. *Earthquake Spectra*, **30**(1): 307-334. https://doi.org/10.1193/021713EQS036M

5 Elwood KJ (2013). "Performance of concrete buildings in the 22 February 2011 Christchurch earthquake and implications for Canadian codes". *Canadian Journal of Civil Engineering*, **40**(3): 1-18. https://doi.org/10.1139/cjce-2011-0564

6 Lu Y, Henry RS, Gultom R and Ma QT (2017). “Cyclic testing of reinforced concrete walls with distributed minimum vertical reinforcement”. *Journal of Structural Engineering*, **143**(5). https://doi.org/10.1061/(ASCE)ST.1943-541X.0001723

7 Almeida J, Prodan O, Rosso A and Beyer K (2017). “Tests on thin reinforced concrete walls subjected to in-plane and out-of-plane cyclic loading”. *Earthquake Spectra*, **33**(1): 323-345. https://doi.org/10.1193/101915EQS154DP

8 Niroomandi A, Pampanin S, Dhakal RP, Soleymani Ashtiani M and Nokes R (2021). “Experimental study on the effects of bi-directional loading pattern on rectangular reinforced concrete walls”. *Earthquake Engineering and Structural Dynamics*, **50**(7): 2010-2030. https://doi.org/10.1002/eqe.3433

9 Dashti F, Dhakal RP and Pampanin S (2017). “Tests on slender ductile structural walls designed according to New Zealand Standard”. *Bulletin of the New Zealand Society for Earthquake Engineering*, **50**(4): 504-516. https://doi.org/10.5459/bnzsee.50.4.504-516

10 Tripathi M, Dhakal RP and Dashti F (2019). “Bar buckling in ductile RC walls with different boundary zone detailing: Experimental investigation”. *Engineering Structures*, **198**: 109544. https://doi.org/10.1016/j.engstruct.2019.109544

11 Shegay AV, Dashti F, Hogan L, Lu Y, Niroomandi A, Seifi P, Zhang T, Dhakal RP, Elwood KJ, Henry RS and Pampanin S (2020). “Research programme on seismic performance of reinforced concrete walls: Key recommendations”. *Bulletin of the New Zealand Society for Earthquake Engineering*, **53**(3): 54-69. https://doi.org/10.5459/bnzsee.53.2.54-69

12 Lu Y and Henry RS (2017). “Minimum vertical reinforcement in RC walls”. *Bulletin of the New Zealand Society for Earthquake Engineering*, **50**(4): 471-481. https://doi.org/10.5459/bnzsee.50.4.471-481

13 Dashti F, Dhakal RP and Pampanin S (2021). “Design recommendations to prevent global OOP instability of rectangular RC ductile walls”. *Bulletin of the New Zealand Society for Earthquake Engineering*, **54**(3): 211-227. https://doi.org/10.5459/bnzsee.54.3.211-227

14 Tripathi M and Dhakal RP (2021). “Designing and detailing transverse reinforcement to control bar buckling in rectangular RC walls”. *Bulletin of the New Zealand Society for Earthquake Engineering*, **54**(3): 228-242. https://doi.org/10.5459/bnzsee.54.3.228-242

15 Aktan AE and Bertero VV (1984). “Seismic response of R/C frame-wall structures”. *Journal of Structural Engineering*, **110**(8): 1803-1821. https://doi.org/10.1061/(ASCE)0733-9445(1984)110:8(1803)

16 Bertero V, Aktan AE, Charney F and Sause R (1984). “Earthquake simulator tests and associated experimental, analytical, and correlation studies of one-fifth scale model”. *ACI Special Publication*, **84**: 375-424.

17 Kabeyasawa T, Shiohara H, Otani S and Aoyama H (1983). “Analysis of the full-scale seven-story reinforced concrete test structure”. *Journal of the Faculty of Engineering: University of Tokyo*, **37**(2): 431-478.

18 Panagiotou M, Restrepo JI and Conte JP (2010). “Shake-table test of a full-scale 7-story building slice. Phase I: Rectangular wall”. *Journal of Structural Engineering*, **137**(6): 691-704. https://doi.org/10.1061/(ASCE)ST.1943-541X.0000332

19 Henry RS, Ingham JM and Sritharan S (2012). "Wall-to-floor interaction in concrete buildings with rocking wall systems." *Annual Conference of the New Zealand Society for Earthquake Engineering*, Christchurch, NZ.

20 Gavridou S (2015). "*Shake-Table Testing and Analytical Modeling of a Full-Scale, Four-Story Unbonded Post-Tensioned Concrete Wall Building*". PhD Dissertation, University of California at Los Angeles, USA.

21 Watkins J, Sritharan S, Nagae T and Henry RS (2017). "Computational modelling of a four storey post-tensioned concrete building subjected to shake table testing". *Bulletin of the New Zealand Society for Earthquake Engineering*, **50**(4): 595-607. https://doi.org/10.5459/bnzsee.50.4.595-607

22 Mitchell D and Paultre P (1994). "Ductility and overstrength in seismic design of reinforced concrete structures". *Canadian Journal of Civil Engineering*, **21**(6): 1049-1060.

23 Nassar AA and Krawinkler H (1991). "*Seismic Demands for SDOF and MDOF Systems*". Report No. 95, Blume Earthquake Engineering Center, Department of Civil Engineering, Stanford University, California, USA.

24 Humar JL and Rahgozar MA (1996). "Concept of overstrength in seismic design". *Eleventh World Conference on Earthquake Engineering*, **639**: 1-8.

25 Elnashai AS and Mwafy AM (2002). "Overstrength and force reduction factors of multi-storey reinforced-concrete buildings". *The Structural Design of Tall Buildings*, **11**(5): 329-351. https://doi.org/10.1002/tal.204

26 CEN (2004). "*European Standard EN 1998-1:2004 Eurocode 8: Design of Structures for Earthquake Resistance, Part 1: General Rules, Seismic Actions and Rules for Buildings*". Comite Europeen deNormalisation, Brussels, Belgium.

27 FEMA-450 (2004). "*NEHRP Recommended Provisions for Seismic Regulations for New Buildings and Other Structures*". Federal Emergency Management Agency, Washington, DC, USA.

28 Standards New Zealand (2006). "*NZS 3101: Concrete Structures Standard*". Standards New Zealand, Wellington, NZ.

29 Standards New Zealand (2004). "*NZS 1170.5: Structural Design Actions. Part 5: Earthquake Actions-New Zealand*". Standards New Zealand, Wellington, NZ, 76 pp.

30 SEAOC Seismology Committee (2006). "*SEAOC Blue Book: Seismic Design Recommendations*". Structural Engineers Association of California, Sacramento, USA.

31 Clough DP (1982). "Considerations in the design and construction of precast concrete diaphragms for earthquake loads". *PCI Journal*, **27**(2): 79-93.

32 Encina E, Lu Y and Henry RS (2016). "Axial elongation in ductile reinforced concrete walls". *Bulletin of the New Zealand Society for Earthquake Engineering*, **49**(4): 305-318. https://doi.org/10.5459/bnzsee.49.4.305-318

33 Peng B, Dhakal RP, Fenwick R, Carr A and Bull D (2011). "Elongation of plastic hinges in ductile RC members: Model development". *Journal of Advanced Concrete Technology*, **9**(3): 315-326. https://www.jstage.jst.go.jp/article/jact/9/3/9_3_315/_pdf

34 Peng B, Dhakal RP, Fenwick R, Carr A and Bull D (2011). "Elongation of plastic hinges in ductile RC members: Model verification". *Journal of Advanced Concrete Technology*, **9**(3): 327-338. https://www.jstage.jst.go.jp/article/jact/9/3/9_3_327/_pdf

35 Mander JB, Priestley MJ and Park R (1988). "Theoretical stress-strain model for confined concrete". *Journal of Structural Engineering*, **114**(8): 1804-1826. https://doi.org/10.1061/(ASCE)0733-9445(1988)114:8(1804)

36 Priestley MJN, Calvi MC and Kowalsky MJ (2007). *Displacement-Based Seismic Design of Structures*. IUSS Press, Pavia, 670 pp.

37 Kazaz İ, Gülkan P and Yakut A (2012). "Deformation limits for structural walls with confined boundaries". *Earthquake Spectra*, **28**(3): 1019-1046. https://doi.org/10.1193/1.4000059

38 Thomsen IV JH and Wallace JW (2004). "Displacement-based design of slender reinforced concrete structural walls-experimental verification". *Journal of Structural Engineering*, **130**(4): 618-630. https://doi.org/10.1061/(ASCE)0733-9445(2004)130:4(618)

39 CSI (2014). "*SAP2000 Ver. 17.1.1: Integrated Finite Element Analysis and Design of Structures Basic Analysis Reference Manual*". Computers and Structures INC, Berkeley, USA.

40 Kolozvari K, Arteta C, Fischinger M, Gavridou S, Hube M, Isakovic T, Lowes L, Orakcal K, Vásquez J and Wallace J (2018). "Comparative study of state-of-the-art macroscopic models for planar reinforced concrete walls". *ACI Structural Journal*, **115**(6): 1637-1657. https://doi.org/10.14359/51710835

41 Kolozvari K, Biscombe L, Dashti F, Dhakal RP, Gogus A, Gullu F, Henry R, Massone L, Orakcal K, Rojas F, Shegay A and Wallace J (2019). "State-of-the-art in nonlinear finite element modeling of isolated planar reinforced concrete walls". *Engineering Structures*, **194**: 46-65. https://doi.org/10.1016/j.engstruct.2019.04.097

42 Chang TL, Lee CL, Carr A, Dhakal RP and Pampanin S (2019). "A new drilling quadrilateral membrane element with high coarse-mesh accuracy using a modified Hu-Washizu principle". *International Journal for Numerical Methods in Engineering*, **119**(7): 639-660. https://doi.org/10.1002/nme.6066

43 Chang TL, Lee CL, Dhakal RP and Carr AJ (2019). "Numerical evaluations of a novel membrane element in simulations of reinforced concrete shear walls". *Engineering Structures*, **199**:109592. https://doi.org/10.1016/j.engstruct.2019.109592

44 Chang TL, Lee CL, Carr AJ and Dhakal RP (2020). "Numerical evaluations of a novel membrane element in response history analysis of reinforced concrete shear walls". *Engineering Structures*, **220**: 110760. https://doi.org/10.1016/j.engstruct.2020.110760

45 Dashti F, Dhakal RP and Pampanin S (2017). "Numerical modeling of rectangular reinforced concrete structural walls". *ASCE Journal of Structural Engineering*, **143**(6): 04017031. https://doi.org/10.1061/(ASCE)ST.1943-541X.0001729

46 Sedgh RE, Dhakal RP and Carr AJ (2015). "State of the art: Challenges in analytical modelling of multi-storey shear wall buildings". *New Zealand Society for Earthquake Engineering Annual Conference*, Rotorua, NZ, pO-15.

47 Sedgh RE (2019). "*Interaction between Structural Walls, Flooring Slabs and Gravity Frames in Reinforced Concrete Buildings*". PhD Dissertation, University of Canterbury, Christchurch, NZ. http://dx.doi.org/10.26021/1699

48 FEMA-695 (2009). "*Quantification of Building Seismic Performance Factors*". Federal Emergency Management Agency, Washington, DC, USA.

49 ATC-40 (1996). "*Seismic Evaluation and Retrofit of Concrete Buildings*". Applied Technology Council, Seismic Safety Commission, Redwood City, California, USA.